BL7U

# Nodeless Superconducting Gap in $A_xFe_2Se_2$ (A=K, Cs) Revealed by Angle-Resolved Photoemission Spectroscopy

Y. Zhang[1], L. X. Yang[1], M. Xu[1], Z. R. Ye[1], F. Chen[1], C. He[1], H. C. Xu[1], J. Jiang[1], B. P. Xie[1], J. J. Ying[2], X. F.Wang[2], X. H. Chen[2], J. P. Hu[3], M. Matsunami[4], S. Kimura[4] and D. L. Feng[1]

[1] *State Key Laboratory of Surface Physics, Advanced Materials Laboratory, and Department of Physics, Fudan University, Shanghai 200433, China*

[2] *Hefei National Laboratory for Physical Sciences at Microscale and Department of Physics, University of Science and Technology of China, Hefei, Anhui 230026, China*

[3] *Department of Physics, Purdue University, West Lafayette, Indiana 47907, USA*

[4] *UVSOR Facility, Institute for Molecular Science and The Graduate University for Advanced Studies, Okazaki 444-8585, Japan*

Pairing symmetry is a fundamental property that characterizes a superconductor. For the iron-based high-temperature superconductors, an s±-wave pairing symmetry has received increasing experimental and theoretical support. More specifically, the superconducting order parameter is an isotropic s-wave type around certain Fermi surface, but it has opposite signs between the hole Fermi surfaces at the zone center and the electron Fermi surfaces at the zone corners.

Recently, a new series of iron-based superconductors, $A_xFe_2Se_2$ (A=K, Cs), has been discovered with relatively high transition temperature of ~30 K [1]. We have conducted angle-resolve photoemission spectroscopy (ARPES) experiment on $A_xFe_2Se_2$ (A=K, Cs) at beamline BL7U [2].

Figure 1 (a) reveal the photo emission intensity map along out-of-plane momentum ($k_z$) in the ΓZAM plane. The cross-sections of the κ and δ Fermi surfaces clearly show weak dispersion along the $k_z$ direction, indicative of a rather two-dimensional electronic structure. The spectral weight of κ increases from Γ to Z, and a small electron pocket could be clearly observed for the κ band around Z [Fig. 1 (b)]. This gives an electron pocket around Z with its residual spectral weight extending towards Γ. However, we emphasize that the size of the κ pocket is much smaller than that of the δ pocket, which is rather $k_z$-independent as illustrated in Fig. 1 (c). The experimental Fermi surface topology clearly shows that there is no hole Fermi surface near the zone centre, and $A_{0.8}Fe_2Se_2$ is indeed the most heavily electron-doped iron-based superconductor by far.

The momentum distribution of superconducting gap is deduced in Fig. 2. The gap of the band around the M point is of the isotropic s-wave type within the experimental uncertainty, which averagely is about 10.3 meV. Further data taken with different photon energies in Fig. 2 (b) indicate such a gap does not vary with the out-of-plane momentum $k_z$. Smaller gap about 7 meV could be observed for the κ band with little $k_z$-dependence.

Our data show that the rather robust superconductivity in such a highly electron-doped iron-based superconductor could mainly rely on the electron Fermi surfaces near M. Thus, the sign change in the s± pairing symmetry driven by the inter-band scattering as suggested in many weak coupling theories becomes conceptually irrelevant in describing the superconducting state here. A more conventional s-wave pairing is probably a better description.

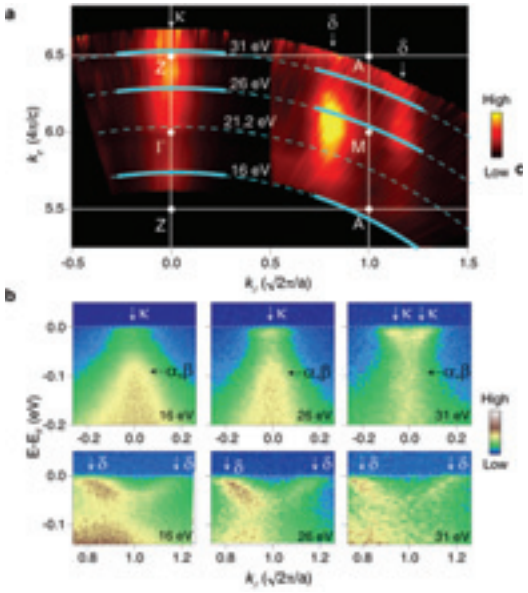

Fig.1. The Fermi surface and band structure as a function of $k_z$ for $K_{0.8}Fe_2Se_2$.

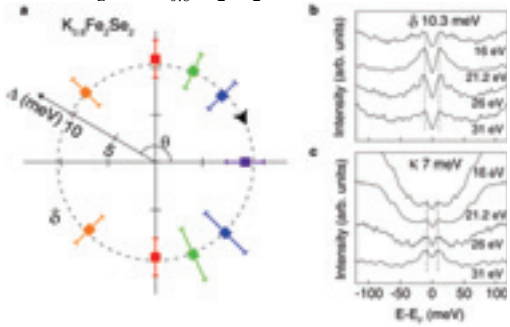

Fig. 2. Momentum dependence of the superconducting gap of $K_{0.8}Fe_2Se_2$.

[1] J. Guo *et al.*, Phys. Rev. B **82** (2010) 180520.
[2] Y. Zhang *et al.*, Nature Materials, **10** (2011) 273.

BL1A

# Characterization of Magnesium in Huntite by an XAFS Method

T. Kurisaki[1], D. Tanaka[1], S. Kokubu[1] and H. Wakita[1,2]

[1] *Department of Chemistry, Faculty of Science, Fukuoka University, Fukuoka 814-0180, Japan*

[2] *Advanced Materials Institute, Fukuoka University Fukuoka 814-0180, Japan*

A huntite was called 'a hanto-ishi' and was used as a pigment of the white in ancient Egypt. This mineral chemical formula is expressed in $CaMg_3(CO_3)_2$. The huntite has very few reports about locality, and it is a rare mineral. However, this mineral is used abundantly in ancient Egypt. On the other hand, the dolomite is a general carbonate that has a similar chemical composition to the huntite. But, the dolomite was not used as a white pigment It is not apparent why the huntite which is a rare mineral was used as a pigment of the white. It is reported that the huntite is produced in Nagasaki. The X-ray absorption spectroscopy is frequently used for steric and electronic structure analyses because it gives good information on the local structure and oxidation state of the absorbing atom [1]. We performed electronic structure analysis of calcium in the huntite using the XAFS method in last year.

In this work, we performed the XANES spectra measurement about various magnesium salts and minerals such as huntite and dolomite. The obtained experimental XANES spectra are analyzed using the calculated theoretical spectra from DV-Xα calculations. The X-ray absorption spectra were measured at BL1A of the UVSOR in the Institute of Molecular Science, Okazaki [2]. The ring energy of the UVSOR storage ring was 750 MeV. Mg K-edge absorption spectra were recorded in the regions of 1275-1380 eV by use of two Beryl crystals. The absorption was monitored by the total electron yield using a photomultiplier. The samples were spread onto the carbon tape on the first photodynode made of CuBe of the photomultiplier.

Figure 1 shows the observed Mg K-edge XANES spectra for the Huntite and Dolomite. The Mg-K XANES spectra of Huntite and Dolomite show different peak profiles at second peaks. This result shows that the magnesium in these minerals has different electronic states. We are going to try to calculate the spectra by DV-Xα molecular orbital calculations. The calculated XANES spectra and the observed XANES spectra of the Huntite and the Dolomite are shown in Fig. 2.

The observed XANES spectra and the calculated XANES spectra showed good agreement. The peak A is estimated to the electron transition (mainly Mg 1s to unoccupied mixed orbital consisting of O 3d, O 3p, O 3s and O 4s). The obtained XANES spectra are analyzed using the calculated spectra from DV-Xα calculations.

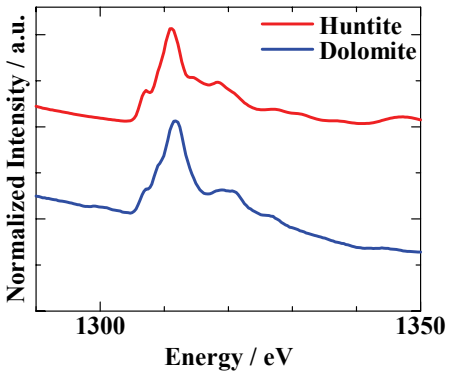


Fig. 1. Observed Mg K-edge XANES spectra of Huntite and Dolomite.

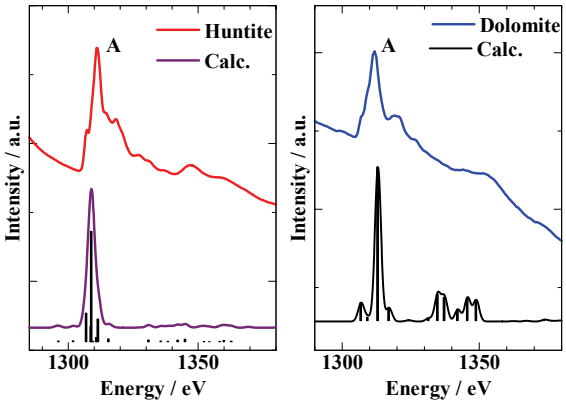


Fig. 2. The comparison of observed XANES spectra with calculated XANES spectra for Mg K-edge.

[1] T. Kurisaki, S. Matsuo, I. Toth and H. Wakita, Anal. Sci. **24** (2008) 1385.

[2] S. Murata, T. Matsukawa, S. Naoè, T. Horigome, O. Matsuodo and M. Watatabe, Rev. Sci. Instrum. **63** (1992) 1309.

BL1B

# Temperature Dependence of Polarized Fundamental Absorption-Edge Spectra of $PbMoO_4$

M. Fujita[1] and M. Itoh[2]

[1] *Japan Coast Guard Academy, Kure 737-8512, Japan*

[2] *Dept. Electrical and Electronic Engineering, Shinshu University, Nagano 380-8553, Japan*

Lead molybdate ($PbMoO_4$) is well known as a superior medium for acousto-optic devices. This material also attracts attention because of its great potential to be used as an effective cryogenic detector for double β decay experiments. The crystal has the scheelite structure with the optical axis along the *c*-axis. Recently we found remarkable dichroism of the lowest exciton band at 3.6 eV in $PbMoO_4$ [1]. In the present study, we have measured the temperature dependence of the fundamental absorption-edge spectra of $PbMoO_4$ crystals with use of polarized light.

$PbMoO_4$ samples were obtained from Furukawa Company. They were grown by the Czochralski technique from the raw materials of PbO of 99.99% purity and $MoO_3$ of 99.9% purity in 1:1 molar ratio, and was purified by three-time crystallization. The thickness of the sample was 2.0 mm.

The absorption spectra for the polarization parallel to the *a*-axis (***E***//***a***) and *c*-axis (***E***//***c***) measured at various temperatures are shown in Figs. 1 (a) and (b), respectively. Distinct dichroism is observed at each temperature. For ***E***//***a***, a weak absorption band is observed as a shoulder superimposed on the tail above 150 K. The band shows significant red shift and becomes remarkable with increasing temperature. Such structure is not observed for ***E***//***c***. It should be noted that the exciton absorption band [1] and the shoulder structure in Fig. 1(a) are both observed distinctly for ***E***//***a***, while they are extremely weak or not discernible for ***E***//***c***. This correspondence suggests that the shoulder structure is attributed to the exciton absorption perturbed by some lattice defects [2].

In contrast to the case of ***E***//***a***, no additional structure is observed in the tail region for ***E***//***c*** at temperatures between 6 and 300 K. In Fig. 2 are plotted the absorption coefficients for ***E***//***c*** in a logarithmic scale. The straight lines fitted to the linear portions of the experimental curves for $T \geq 100$ K converge to a point. This fact indicates that the Urbach rule, $\alpha = \alpha_0 \exp\{-\sigma(E_0-E)/k_BT\}$, holds for $PbMoO_4$ as in the case of $PbWO_4$ [3]. The parameters of the conversing point are obtained as $\alpha_0 = 1.5\times10^4$ cm$^{-1}$ and $E_0 = 3.52$ eV. The steepness parameters $\sigma$ at $T \geq 100$ K are plotted by open circles in the inset in Fig. 2. The solid curve in the inset shows the best fit of the equation, $\sigma(T) = \sigma_0(2k_BT/\hbar\omega)\tanh(\hbar\omega/2k_BT)$ to the data points with the high-temperature steepness parameter $\sigma_0 = 0.67$ and average photon energy $\hbar\omega = 26$ meV.

An exciton in three-dimensional lattices becomes self-trapped and gives rise to a luminescence band with large Stokes shift, when the value of $\sigma_0$ is smaller than the critical value $\sigma_c = 1.50$. The present value of $\sigma_0$ is considerably smaller than this critical value, indicating that the exciton-phonon coupling is strong in $PbMoO_4$. In fact, the intrinsic luminescence due to self-trapped excitons in $PbMoO_4$ is observed with a peak at around 2.3 eV when excited with light of the photon energies above 3.3 eV. The large Stokes shift (~ 1.0 eV) of the intrinsic luminescence band is in satisfactorily agreement with the above conclusion on the strong exciton-phonon coupling in $PbMoO_4$.

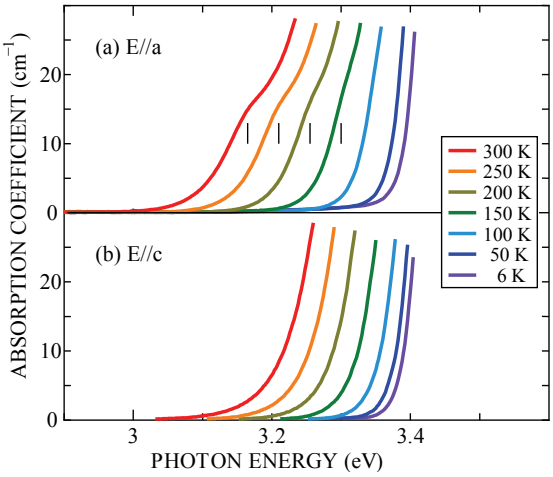


Fig. 1. Absorption-edge spectra of $PbMoO_4$ at various temperatures for (a) ***E***//***a*** and (b) ***E***//***c***.

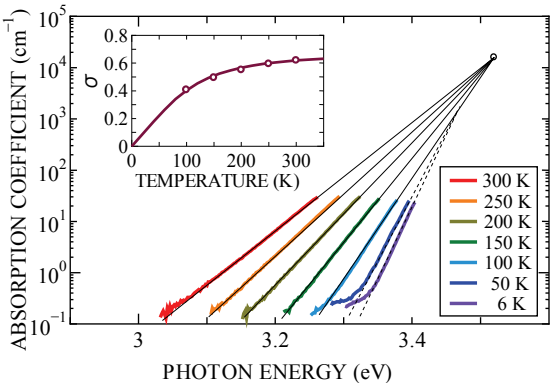


Fig. 2. Logarithmic plot of the absorption spectra for ***E***//***c***. In the inset is shown the temperature dependence of $\sigma$.

[1] M. Fujita *et al.*, Phys. Status Solidi B **247** (2010) 405.

[2] M. Fujita and M. Itoh, Phys. Status Solidi B **247** (2010) 2240.

[3] M. Itoh *et al.*, Phys. Status Solidi B **231** (2002) 595.

BL1B

# Luminescence Properties of KCl:$Ag^-$ Crystals under the Excitation around the Fundamental Absorption Edge

T. Kawai[1] and T. Hirai[2]

[1]*Graduate School of Science, Osaka Prefecture University, Sakai 599-8531, Japan*

[2]*Faculty of Science and Engineering, Ritsumeikan University, Kusatsu 525-8577, Japan*

In KCl crystals containing iodine ions as hetero halogen ions, the absorption bands due to the $I^-$ ions are observed around the fundamental absorption edge of the KCl crystals. The excitation on these absorption bands induces the several luminescence bands due to the localized exciton [1-3]. Among these luminescence bands, the luminescence bands observed in the visible energy region are called the BG and B bands and are attributed to the radiative decay from the relaxed exciton state which consists of a hole localized on a pair of an iodine and chlorine anion and a bound electron, $[(Cl\ I)^- + e^-]$.

In this study, we have investigated luminescence properties of KCl crystals doped with $Ag^-$ centers under the excitation around the fundamental absorption edge. Since the $Ag^-$ anions doped in alkali halide crystals are substituted for the halogen ions, the $Ag^-$ anions would be regarded as pseudo halogen ions. Therefore, the localized excitons related with the $Ag^-$ ions would be existed in the same way as the localized excitons in KCl:I crystals.

Figure 1 shows the luminescence spectra of KCl:$Ag^-$ crystals at 10 K, which are measured at BL1B of the UVSOR facility. Under the excitation on the various energies between 6.42 and 7.21 eV, the luminescence band peaking at 2.91 eV is observed. The 2.91 eV luminescence band is attributed to the radiative transition from the relaxed excited state of $^3T_{1u}$ in the $Ag^-$ center and is called the A' luminescence band [4, 5]. The excitation on 8.26 eV above the intrinsic exciton band of KCl crystals brings about a broad luminescence band at 2.30 eV, which is ascribed to the intrinsic STE in KCl single crystals [6]. It should be noted that a broad luminescence band having a halfwidth of 0.52 eV is observed at 2.60 eV under the excitation on the energy region between 6.66 and 7.21 eV, in addition to the A' luminescence band. The excitation spectra for the 2.60 eV and STE luminescence bands are shown in the insert of Fig. 1. The excitation spectrum for the STE luminescence band exhibits the sharp response at 7.65 and 8.27 eV and is consistent with that reported previously [6]. On the other hand, the excitation spectrum for the 2.60 eV luminescence band exhibits the sharp responses at 6.70, 7.14, and 7.59 eV.

The 2.60 eV luminescence band in KCl:$Ag^-$ is very similar to the BG luminescence band in KCl:I in the energy position and lineshape [1-3]. The excitation spectrum for the 2.60 eV luminescence band exhibits three sharp responses in the energy region between 6.70 and 7.60 eV. The excitation spectrum for the BG luminescence band in KCl:I also has the three responses in the same energy region [1-3]. The similarity between them leads us to the idea that the 2.60 eV luminescence band in KCl:$Ag^-$ has it's origin in the two-center type localized exciton such as $[(Ag\ Cl)^- + e^-]$.

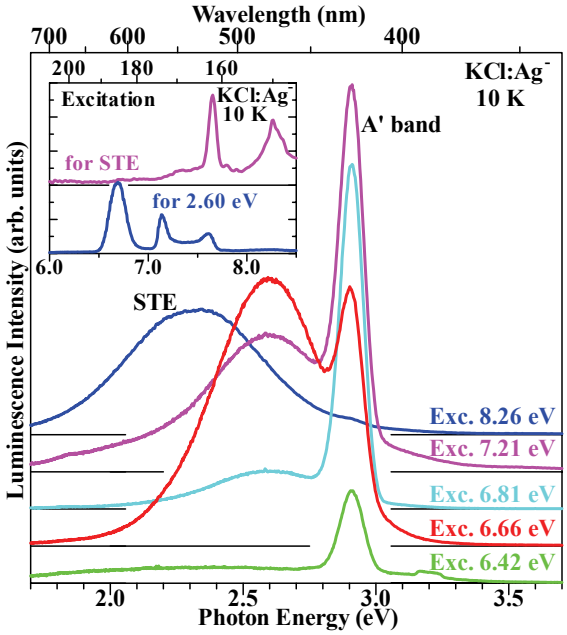


Fig. 1. Luminescence spectra of KCl:$Ag^-$ crystals under the excitation around the fundamental absorption edge. Inset is excitation spectra for the STE and 2.60 eV luminescence bands.

[1] K. Kan'no, M. Itoh and Y. Nakai, J. Phys. Soc. Jpn. **47** (1979) 915.

[2] T. Higashimura, H. Nakatani, M. Itoh, K. Kan'no and Y. Nakai, J. Phys. Soc. Jpn. **53** (1984) 1878.

[3] A. Ohno and N. Ohno, Phys. Status Solidi C **8** (2011) 112.

[4] K. Kojima, S. Shimanuki, M. Maki and T. Kojima, J. Phys. Soc. Jpn. **28** (1970) 1227.

[5] W. Kleemann, Z. Physik **249** (1971) 145.

[6] K. Kan'no, T. Matsumoto and Y. Kayanuma, Pure & Appl. Chem. **69** (1997) 1227.

BL1B

# Optical Study in the Vacuum-Ultraviolet Energy Region of $BaFe_2As_2$

M. Nakajima[1,2,3], K. Kihou[2,3], C. H. Lee[2,3], A. Iyo[2,3], H. Eisaki[2,3] and S. Uchida[1,3]

[1]*Department of Physics, University of Tokyo, Tokyo 113-0033, Japan*

[2]*National Institute of Advanced Industrial Science and Technology, Tsukuba 305-8568, Japan*

[3]*JST, Transformative Research-Project on Iron Pnictides (TRIP), Tokyo 102-0075, Japan*

## Introduction

The parent compounds of iron-arsenide superconductors, with $BaFe_2As_2$ as a representative example, are unique metals which exhibit a structural phase transition accompanied or followed by a magnetic phase transition. The magnetostructural state has attracted much attention as a proximate phase to a superconducting phase. To elucidate the mechanism of superconductivity in iron-based compounds, it is important to investigate the electronic properties in the normal state as well as those in the superconducting state.

Optical spectroscopy is one of the most useful methods for investigating the electronic dynamics in solids. If reflectivity is obtained for a wide energy range, optical conductivity can be derived through the Kramers-Kronig (K-K) transformation of the reflectivity spectrum. In this work, we measured reflectivity in the vacuum-ultraviolet (VUV) region of $BaFe_2As_2$. Reflectivity measurement in this energy region is necessary to obtain reliable optical conductivity for multi-band/orbital systems such as iron-pnictides or cuprates [1], since a number of intraband and interband excitations overlap in the same energy region and extend up to 10 eV or higher.

## Experimental

Single crystals of $BaFe_2As_2$ were synthesized by a self-flux method [2]. The in-plane reflectivity spectrum in the VUV region between 4 and 35 eV was measured at room temperature using a Seya-Namioka-type grating at BL1B of UVSOR facility. The optical conductivity spectrum was obtained via K-K transformation of the measured reflectivity spectrum connected to the lower-energy one.

## Results and Discussion

The in-plane reflectivity spectrum up to 32 eV is shown in Fig. 1. The reflectivity shows good coincidence with the result measured in the laboratory. Three distinct reflectivity edge appear at ~ 1, ~ 10, and ~ 25 eV. Each edge indicates the end point of a series of intraband or interband excitations.

Figure 2 shows the conductivity spectra obtained by various extrapolations above 4.5 eV. If we use conventional extrapolation schemes for the K-K transformation, the obtained conductivity appreciably deviates from the present result, particularly in the region higher than 0.3 eV. Thus, the measurement in the VUV region is essential for quantitative analysis.

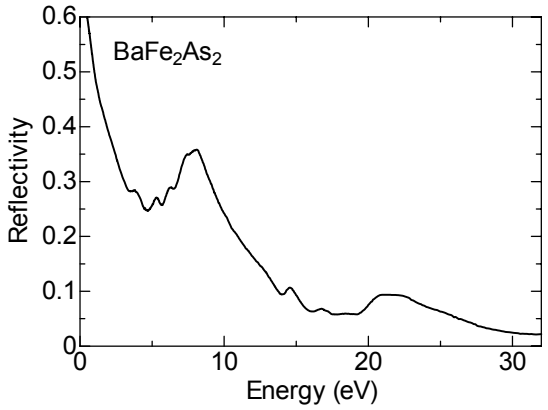


Fig. 1. Reflectivity spectrum of $BaFe_2As_2$ measured at room temperature in the energy range up to 32 eV.

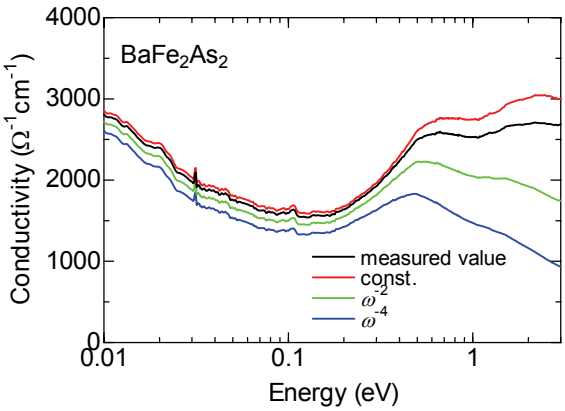


Fig. 2. Kramers-Kronig transformed optical conductivity spectra for various high-energy extrapolations.

[1] S. Tajima *et al.*, J. Opt. Soc. Am. B **6** (1989) 475.
[2] M. Nakajima *et al.*, Phys. Rev. B **81** (2010) 104528.

BL1B

# Identification of $Cr^{3+}$ Impurity Contained in $YAlO_3$ by Photoluminescence

K. Nakahara and Y. Ohki

*Dept. Electrical Engineering and Bioscience, Waseda University, Tokyo 169-8555, Japan*

## Introduction

Yttrium aluminate ($YAlO_3$) has been attracting much attention as a promising candidate for a gate insulator in advanced metal-oxide-semiconductor devices [1]. By analyzing photoluminescence (PL) properties of $YAlO_3$, we have been examining the localized states present in the band gap that are assumed to cause leakage current.

## Experimental

The samples examined are $YAlO_3$ (100) single crystals grown by the Czochralski method and $YAlO_3$ thin films prepared by a spin-coating method. The films were annealed in oxygen at designated temperatures between 600 and 1000 ºC. Using synchrotron radiation under multibunch operation at the BL1B line of UVSOR Facility as a photon source, PL spectra were measured at 10 K. Crystallization of thin films were confirmed by in-plane X-ray diffraction (XRD) measurements.

## Results and Discussion

Figure 1 shows PL spectra induced by 6.4 eV photons, obtained at 10 K for the crystal and the films deposited and annealed on Si substrates. The crystal sample has PL peaks at 1.65 and 1.70 eV. On the other hand, the two PL peaks are similar to those of R-lines of $Cr^{3+}$ ions in Cr-doped $YAlO_3$ [2]. The films annealed at 600, 700 and 800 ºC have no PL peaks, while those annealed at 900 and 1000 ºC have PL peaks at 1.70, 1.75 and 1.79 eV. Similar differences in peak energy between the crystal and the deposited film are also seen in $LaAlO_3$ thin films deposited on different substrates [3], which is possibly due to the lattice distortion.

The XRD patterns shown in Fig. 2 indicate that the films annealed at 900 °C or higher are polycrystalline, while those annealed at 600, 700 and 800 °C are amorphous. As indicated by the broken lines, the two large peaks almost agree with those that should be assigned to $YAlO_3$, and subtle differences would be due to lattice distortion. However, the presence of other small peaks suggests that $Y_3Al_5O_{12}$ and $Y_4Al_2O_9$ are included in the films.

These results indicate that the PL is caused by the crystallization and that the corresponding spin-forbidden transition in $Cr^{3+}$ becomes possible owing to spin-orbit mixing induced by the crystal field [3]. Therefore, there is a possibility that the present $YAlO_3$ samples contain $Cr^{3+}$ ions as an impurity. Detection of $Cr^{3+}$ ions by inductively coupled plasma atomic emission spectrometry (ICP-AES) failed, indicating that the $Cr^{3+}$ ion content in the present samples is below 1 ppm.

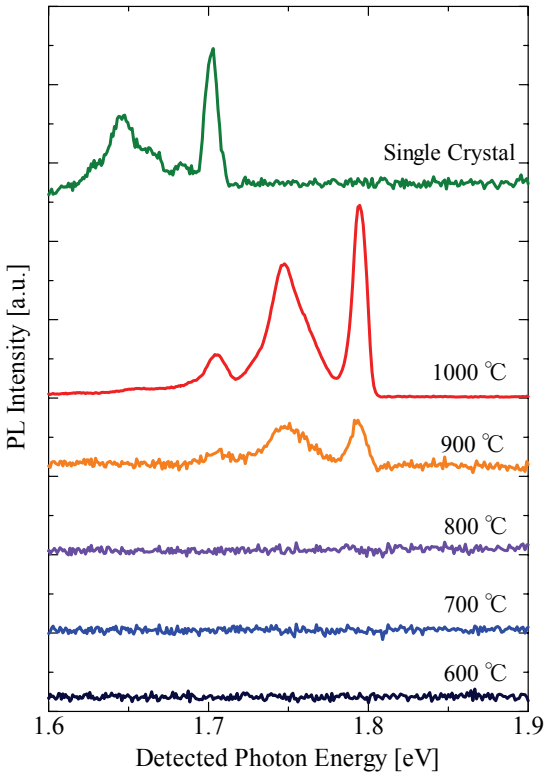


Fig. 1. PL spectra induced by 6.4 eV photons in $YAlO_3$.

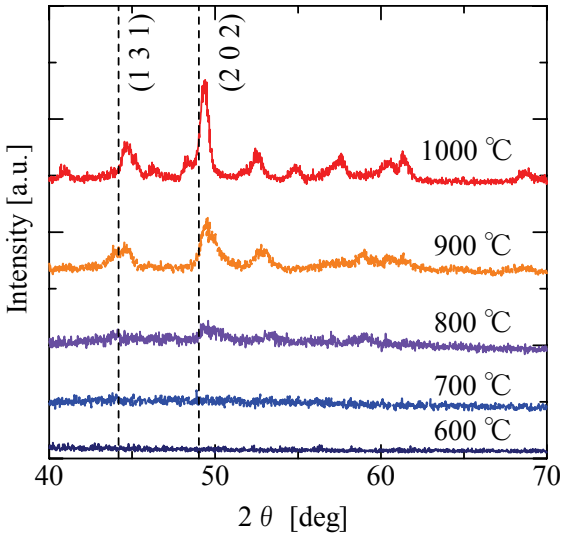


Fig. 2. In-plane XRD patterns of $YAlO_3$ thin films.

[1] S. A. Shevlin *et al.*, Phys. Rev. Lett. **94** (2005) 146401.
[2] M. Yamaga *et al.*, J. Phys.: Condens. Matter **5** (1993) 8097.
[3] E. Hirata *et al.*, Jpn. J. Appl. Phys. **49** (2010) 091102.

BL1B

# Relaxed Exciton Luminescence of KCl Heavily Doped with KI

A. Ohno and N. Ohno

*Graduate School of Engineering, Osaka Electro-Communication University, Neyagawa, Osaka 572-8530, Japan*

Extensive studies have been made on luminescence arising from localized relaxed excitons in KCl containing iodine impurities. Stimulation in iodine absorption bands of dilute $I^-$-doped KCl (KCl:I) produces two characteristic luminescence bands under excitation with UV light or with X-rays at low temperatures. These luminescence bands have been well explained in terms of localized relaxed excitons at $ICl^-$ molecule ($I^-$ monomer) and a complex of two iodine ions ($I^-$ dimer), respectively [1-3]. However, optical and luminescence properties of heavily doped KCl:I crystals have not been examined sufficiently for applying to highly efficient scintillation material.

Single crystals of KCl:I were grown by the Bridgeman method from reagent grade KCl added with an appropriate amount of KI. The obtained crystals were transparent up to 5 mol %. The optical measurements were made at 6 K.

The luminescence spectra excited with photons near the exciton absorption region of KCl were almost the same as those of the previous studies; two luminescence bands peaking at 2.64 eV (monomer emission) and 4.64 eV (dimer emission) at 6 K. Photoexcitation spectra detected at 4.64 eV for various KI mol % of KCl:I crystals are shown in Fig. 1. The each spectrum has been normalized at unity at the maximum. As can be seen clearly, the excitation peaks at 6.46 and 7.07 eV for the 0.01 mol % crystal move toward the lower energy side with increasing KI concentration. The low energy shift of these excitation bands suggests that there coexist dimers, trimers and lager sizes of $I^-$ ions (KI cluster) in heavily doped KCl:I crystal [1].

The luminescence energies of the trimers and clusters of $I^-$ ions in heavily doped KCl:I crystals are expected to be different from that of $I^-$ dimers. We have examined the photoluminescence spectra excited at various photon energies. The results for 3 mol % crystal are shown in Fig. 2. It is clearly confirmed that the peak energy of the luminescence band moves from 4.62 eV excited at 6.46 eV to 4.32 eV at 5.90 eV. These luminescence bands are supposed to be the composite bands due to radiative annihilation of the relaxed exciton at dimers, trimers and clusters of $I^-$ ions.

In KCl:I crystals containing KI above 1 mol %, there exists a small amount of dimer centers as compared with monomers, and moreover the amount of trimers and clusters of KI is supposed to be extremely smaller than those of monomers and dimers. However, the luminescence intensities of such large-sized centers are found to be comparable with that of the dimer emission. This fact suggests that the excitons trapped in KI clusters in heavily doped KCl:I crystals would give the high luminescence efficiency. The similar mechanism has been reported in CsI:Na system [4], where the observed luminescence enhancement originates from self-trapped excitons in NaI nanoparticles in host crystals.

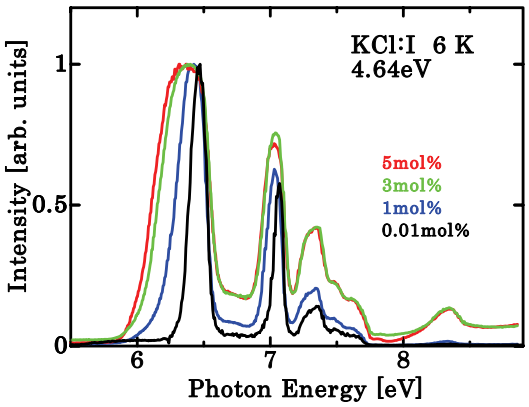


Fig. 1. Photoexcitation spectra of KCl:I crystals detected at 4.64 eV for various KI mol % at 6 K.

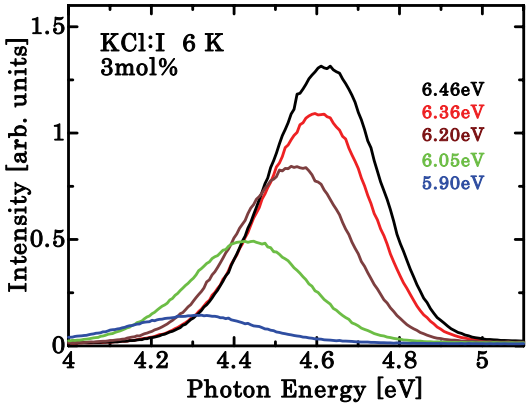


Fig. 2. Photoluminescence spectra of KCl:I (3 mol %) excited at various photon energies at 6 K.

[1] N. Nagasawa, J. Phys. Soc. Jpn. **27** (1969) 1535.
[2] K. Toyoda, K. Nakamura and Y. Nakai, J. Phys. Soc. Jpn. **39** (1975) 994.
[3] K. Kan'no, M. Itoh and Y. Nakai, J. Phys. Soc. Jpn. **47** (1979) 915.
[4] M. Nakayama, N. Ando, T. Miyoshi, J. Hirai and H. Nishimura, Jpn. J. Appl. Phys. **41** (2002) L263.

BL1B

# Optical Study of the Current-Induced Mott Transition in $Ca_2RuO_4$

R. Okazaki[1], Y. Nishina[1], Y. Yasui[1], I. Terasaki[1], F. Nakamura[2], Y. Kimura[2], M. Sakaki[2] and T. Suzuki[2]

[1]*Department of Physics, Nagoya University, Nagoya 464-8602, Japan*
[2]*ADSM, Hiroshima University, Higashi-Hiroshima 739-8530, Japan*

The Mott insulating state, which is driven by the Coulomb interaction $U$, has attracted increasing research interests since it manifests a significance of many-body effects in condensed matter physics. Various exotic electronic states emerge in the vicinity of the Mott insulating phase as seen in high-$T_c$ cuprates and organic conductors.

The 4*d*-electron transition metal oxide $Ca_2RuO_4$ provides various interesting phenomena around the Mott insulating phase. Systematic isovalent Sr-doping study revealed that the ground state of $Ca_{2-x}Sr_xRuO_4$ changes from the antiferromagnetic Mott insulator ($x = 0$) to the spin-triplet superconductor ($x = 2$) [1]. Pressure study also indicates the wide variety of electronic ground states [2].

Very recently, Nakamura *et al.* reported the electric-field-induced Mott transition in $Ca_2RuO_4$ by applying relatively low electric field of ~ 50 V/cm at room temperature [3, 4]. Furthermore the current -induced metallic state persists down to $T = 4.2$ K and the ferromagnetic (FM) order emerges below $T \sim 15$ K, which is reminiscent of the pressure-induced FM state [2]. The origin of this current-induced electronic state is still an open question.

To shed further light on a nature of this nonequilibrium electronic state, we have investigated the optical property of the Mott insulating phase in $Ca_2RuO_4$ under external electrical currents. We used the beam line BL1B in UVSOR facility to measure the reflectivity spectra of $Ca_2RuO_4$ in an energy region of 2 – 30 eV, which enables us to evaluate the optical conductivity through the Kramers-Kronig (KK) analysis. The reflectivity spectra of $Ca_2RuO_4$ single crystals measured at room temperature with different currents are shown in Fig. 1. We find an increase of the reflectivity by the currents in low-energy region, as well as several pronounced peaks corresponding the interband transitions as reported in previous optical studies [5]. Figure 2 shows the optical conductivity spectra of $Ca_2RuO_4$ transformed by the KK analysis. An optical gap decreases as a function of the external currents, implying a possible current-induced metallic state in $Ca_2RuO_4$. We are now developing an evaluation of self-heating effects under the large external currents.

[1] S. Nakatsuji and Y. Maeno, Phys. Rev. Lett. **84** (2000) 2666.
[2] F. Nakamura *et al.*, Phys. Rev. B **65** (2002) 220402(R).
[3] M. Sakaki *et al.*, JPS meeting (2010) 20pPSA-28; Y. Kimura *et al.*, (2010) 24aPS-3.
[4] F. Nakamura *et al.*, submitted.
[5] J.S. Lee *et al.*, Phys. Rev. Lett. **89** (2002) 257402; J.H. Jung *et al.*, **91** (2003) 056403.

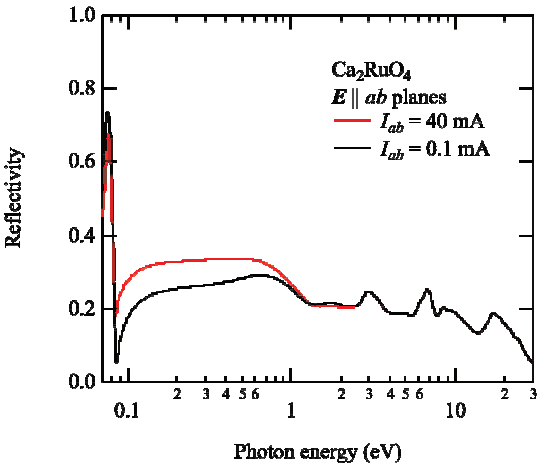


Fig. 1. Reflectivity spectra of $Ca_2RuO_4$ single crystal measured at room temperature with external currents for $\boldsymbol{I} \parallel ab$. The electric field of incident light is parallel to the *ab* planes.

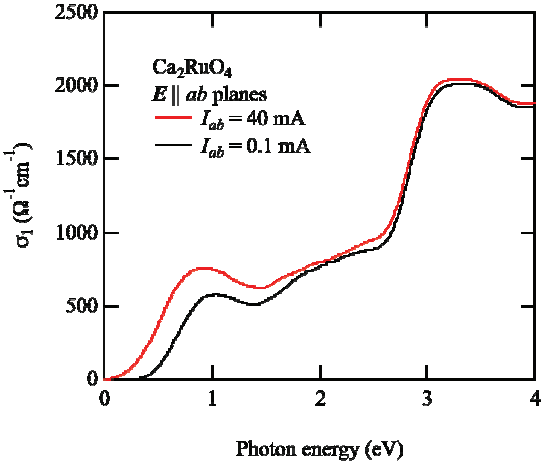


Fig. 2. Optical conductivity $\sigma_1$ of $Ca_2RuO_4$ obtained from the Kramers-Kronig transformation of the reflectivity spectra.

BL1B

# Metal-Insulator Transition in $V_{1-x}W_xO_2$

J. S. Lee[1], K. Shibuya[2], M. Kawasaki[1,2] and Y. Tokura[1,2,3]

[1]*Department of Applied Physics and Quantum Phase Electronics Center (QPEC), University of Tokyo, Tokyo 113-8656, Japan*

[2]*Correlated Electron Research Group (CERG) and Cross-Correlated Materials Research Group (CMRG), ASI, RIKEN, Wako 351-0198, Japan*

[3]*Multiferroics Project, ERATO, Japan Science and Technology Agency (JST), Tokyo 113-8656, Japan*

The metal-insulator transition in $VO_2$ takes place at around 340 K accompanying the structural transition from high-temperature rutile to low-temperature monoclinic phases. Dimerization of V ions occurs in the latter with a tilting of the V–V bond from *c*-axis. 3*d* electrons localize on V sites forming spin singlet dimers. The driving mechanism of the metal-insulator transition has long been argued whether Mott–Hubbard or Peierls transitions. It has been recently suggested that both mechanisms are active and thus the transition is viewed as a many-body Peierls type.

From the viewpoint of device application, dramatic change in electrical resistivity as well as infrared transmission across the transition above room temperature makes $VO_2$ potentially useful for optical, electrical, and electro-optical switches by exploiting the phase control through the electron injection into pure $VO_2$ by electric field or light absorption. There has been an enduring interest in controlling the metal-insulator transition temperature ($T_{MI}$) of $VO_2$ by chemical substitution. Electron doping with use of higher valence elements such as W, Mo, and Nb was shown to reduce the transition temperature. Among them, W is known to be the most effective, reducing the transition temperature by 21–28 K/at.%. The valence of W was confirmed to be 6+, which corresponds to adding two electrons per W atom. However, physical properties of electron-doped $VO_2$ are not well understood because only few studies have been carried out in single crystals.

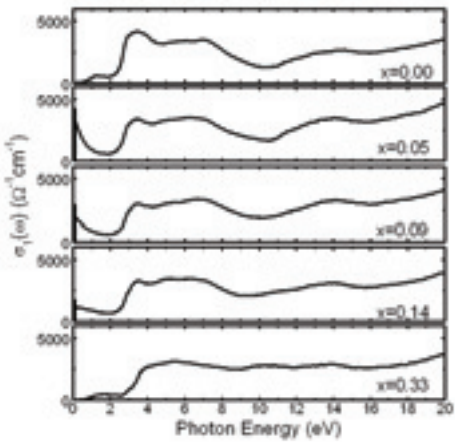


Fig. 1. Optical conductivity spectra $\sigma_1(\omega)$ of $V_{1-x}W_xO_2$ obtained at the room temperature.

Here, we have investigated optical properties of solid-solution $V_{1-x}W_xO_2$ epitaxial films in a wide range of doping concentration ($0 \leq x \leq 0.33$). We found there are systematic variations of the optical conductivity spectra in the high energy region (as shown in Fig. 1). Detailed examination of the optical gap reveals that the ground state changes from the insulator, to metal, and to insulator as $x$ (the W content) increases (upper panels in Fig. 2). As a signature of the dimerization of V ions there appear the splitting of the phonon around 300 $cm^{-1}$ for the pure $VO_2$. As $x$ increases, the splitting becomes less prominent and is absent for $x$=0.33 (lower panels in Fig. 2). This indicates that while the insulating state for $x$ = 0.0 is closely related to the Peierls instability, that for $x$ = 0.33 can be understood by considering purely the electron-correlation.

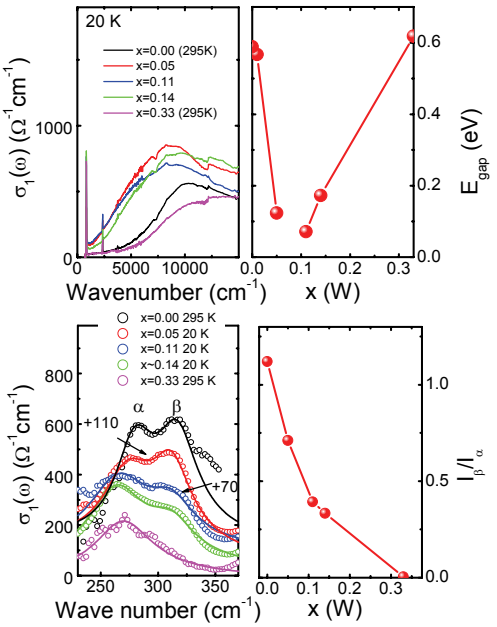


Fig. 2. Left panels: the optical conductivity spectra up to the visible region (upper) and in the far-infrared region (lower). Right panels: doping-dependences of the optical gap energy (upper) and the intensity ratio of two phonon modes (lower).

[1] F. J. Morin, Phys. Rev. Lett. **3** (1959) 34.
[2] J. B. Goodenough, J. Solid State Chem. **3** (1971) 490.
[3] K. Shibuya et al., Appl. Phys. Lett. **96** (2010) 022102.

BL1B

# Analysis of 4*f*-5*d* Excitation Spectra of $Pr^{3+}$-Doped $SrY_2O_4$

S. Watanabe[1], Y. Ichikawa[2], M. Yoshino[2], T. Yamada[2] and T. Nagasaki[3]

[1] *Venture Business Laboratory, Nagoya University, Nagoya 464-8603, Japan*

[2] *Department of Materials, Physics and Energy Engineering, Graduate School of Engineering, Nagoya University, Nagoya 464-8603, Japan*

[3] *EcoTopia Science Institute, Nagoya University Nagoya 464-8603, Japan*

Trivalent praseodymium ($Pr^{3+}$)-doped oxides have been widely studied for application as a luminescent material in devices such as solid-state lasers and phosphors. Because of strong recent desire for luminescent materials in high-energy regions, the $4f^2$-$4f^15d^1$ transitions of $Pr^{3+}$ in wide band-gap host crystals have drawn attention for potential application as UV and VUV phosphors.

We make a report of the analysis of the emission and excitation spectra for $Pr^{3+}$-doped $SrY_2O_4$. The $Pr^{3+}$-doped $SrY_2O_4$ sample was prepared by the solid-state reaction at 1323 K and identified as single phase by x-ray diffraction measurement. The concentration of $Pr^{3+}$ ion in the sample was 3 mol%. The excitation spectrum at 10 K was measured monitoring the emission at 516 nm.

In addition, we also analyzed the spectra based on first-principles calculations for multiplet energy and absorption spectrum using the 4-component relativistic configuration interaction (CI) method [1, 2]. This calculation method has been successfully applied to analysis of the multiplet energy levels and optical spectrum between the multiples for impurity ions in host crystals. The $SrY_2O_4$ host crystal has three cation sites, which are Y1 site, Y2 site and Sr site. The occupied sites of the $Pr^{3+}$ ions were analyzed by comparison between the experimental spectrum and theoretical spectra. The solution energies of $Pr^{3+}$ into the host crystal were also estimated by first-principles band calculations. These calculations were performed using VASP code [3].

The calculated solution energies of $Pr^{3+}$ into $SrY_2O_4$ host crystal were 0.11 eV for Y1 site, 0.31 eV for Y2 site and 0.64 eV for Sr site, respectively, at oxidation limits. For the substitution in Sr site by $Pr^{3+}$ ion, the oxygen vacancy in host crystal, $SrY_2O_4$, required for the charge compensation. Therefore it is natural that the solution energy of $Pr^{3+}$ into the Sr site was much higher than the solution energy of $Pr^{3+}$ into other two sites.

Figure 1 shows the experimental excitation spectrum and theoretical absorption spectra. The peaks A – F were observed in the experimental spectrum. The peak E originates in the fundamental absorption of the $SrY_2O_4$ host crystal. The theoretical spectra were calculated with three models, which were occupied three sites mentioned above, respectively (Y1, Y2 and Sr site). While the intensity of the experimental excitation spectrum is not directly compared with the theoretical absorption spectra, relative peak energy can compared between each spectra. The absorption of the $Pr^{3+}$ ions in all three sites , Y1, Y2 and Sr site, contributed to the peaks A, B and C. On the other hand, the peak D can clearly attributed the absorption of $Pr^{3+}$ in Sr site and the broad peak F can attributed the absorption of $Pr^{3+}$ in Y1 and Y2 site.

Consequently, we can conclude that the $Pr^{3+}$ ions occupied in all three sites, Y1, Y2 and Sr site.

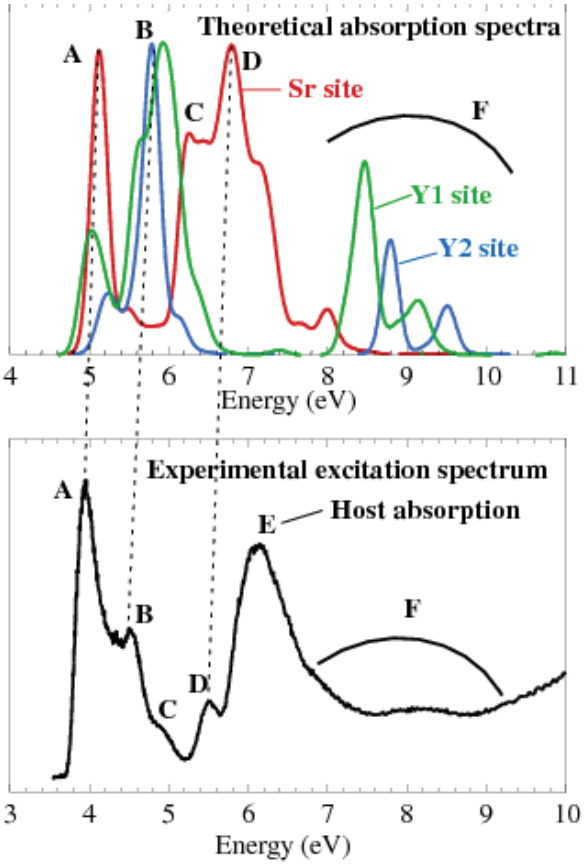


Fig. 1. Experimental excitation spectrum and theoretical absorption spectra of $Pr^{3+}$-doped $SrY_2O_4$ materials.

[1] K. Ogasawara, T. Iwata, Y. Koyama, T. Ishii, I.Tanaka and H. Adachi, Phys. Rev. B **64** (2001) 143.
[2] S. Watanabe, K. Ogasawara, M. Yoshino and T. Nagasaki, Phys. Rev. B **81** (2010) 125128.
[3] G. Kresse and D. Joubert, Phys. Rev. B **59** (1999) 1758.

BL4B

# Charge State Analysis of Co Ions in $Pr_{1-x}Sr_xCoO_{3-\delta}$

T. Yoshioka, H. Kanamori and T. Yamamoto
*Faculty of Science and Engineering, Waseda University, Tokyo 169-8555, Japan*

## Introduction

Perovskite-type cobalt oxides $R_{1-x}A_xCoO_{3-\delta}$ (R and A are rare-earth and alkaline-earth ions, respectively) have been extensively studied, because of their unique electronic and magnetic properties such as colossal magnetoresistance and metal-insulator transition [1-3]. In order to understand such properties, it is essential to know the charge state, i.e., valence, of Co ions in these materials. When the alkaline-earth ion is incorporated into $PrCoO_3$, i) valence of Co ions controls the system, i.e., from $Co^{3+}$ to $Co^{4+}$ or ii) oxygen vacancy is created, to keep the system electrically neutral. However, these mechanisms of charge compensation have not yet been fully understood. Then the charge state analysis of Co ions in $Pr_{1-x}Sr_xCoO_{3-\delta}$ are carried out here by the Co-$L_{2,3}$ X-ray absorption near-edge structure (XANES) measurements changing a concentration of Sr (x=0, 0.1, 0.3, 0.5, 0.7) .

## Experiments

$Pr_{1-x}Sr_xCoO_{3-\delta}$ samples were synthesized by the conventional solid-state reaction method. Co-$L_{2,3}$ XANES spectra were collected at BL4B in UVSOR by the total electron yield (TEY) method. All the sample powders were mounted on the first Be-Cu dinode using the carbon adhesive tape. The incident beam was monochromatized by the varied-line-spacing plane grating (800 lines/mm). The energy resolution of the incident beams, E/ΔE was set to 3000 by tuning the slit height settled at the upper and lower reaches of the grating.

## Results

Prior to the XANES analysis, all the samples were characterized by the X-ray diffraction (XRD). No extra peaks were found in the observed XRD patterns except for those of the perovskite structured $Pr_{1-x}Sr_xCoO_{3-\delta}$, which yield the $Pr_{1-x}Sr_xCoO_{3-\delta}$ crystallizes orthorhombic perovskite structure (Pbnm) at ambient condition.

Observed Co-$L_3$ XANES spectra of $Pr_{1-x}Sr_xCoO_{3-\delta}$ are shown in Fig. 1, in which fine structure of Co-$L_3$ XANES spectra of $Pr_{1-x}Sr_xCoO_{3-\delta}$ changes as increment of the concentration of doped $Sr^{2+}$ ions. From the deconvolution of the experimental spectra using the Gaussian function (red lines in Fig. 1), it is found that relative intensity of peak A to B increases as increment of Sr concentration (Fig. 2). These experimental results suggest that electronic structure of Co ions in $Pr_{1-x}Sr_xCoO_{3-\delta}$ changes continuously as increment of Sr concentration.

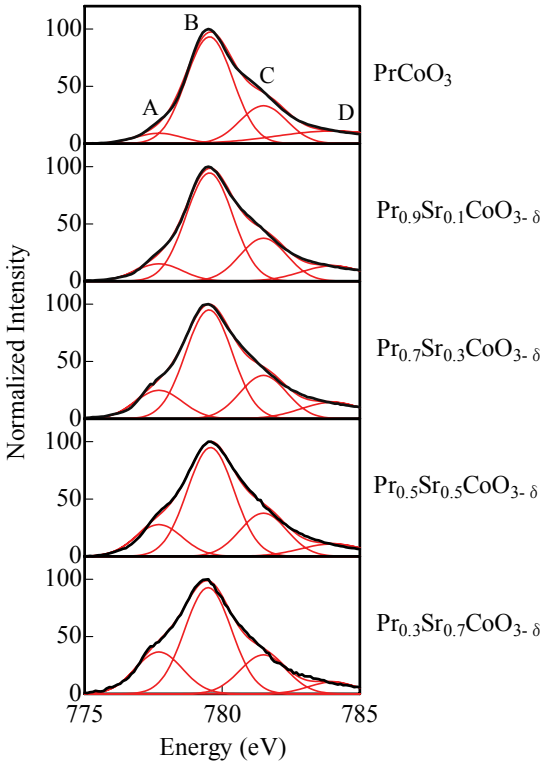


Fig. 1. Observed Co-$L_3$ XANES spectra of $Pr_{1-x}Sr_xCoO_{3-\delta}$ .

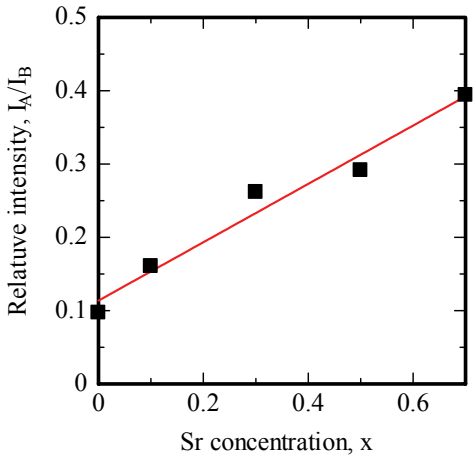


Fig. 2. Relative intensity of peak A to B as a fnction of Sr concentration, x, in $Pr_{1-x}Sr_xCoO_{3-\delta}$ .

[1] S. Tsubouchi *et al.*, Phys. Rev. B **69** (2004) 144406.
[2] H. Masuda *et al.*, J. Phys. Soc. Jpn. **72** (2003) 873.
[3] V. Golovanov and L. Mihaly, Phys. Rev. B **53** (1996) 8207.

BL5U

# Electronic Structure of Heusler-Type Alloys $Fe_{2-y}M_yVAl$ ($M$ = Co, Rh, Ir)

S. Harada[1], M. Kato[1], S. Yagi[1], K. Soda[1], Y. Nishino[2] and H. Miyazaki[3]

[1]*Graduate School of Engineering, Nagoya University, Nagoya 464-8603, Japan*

[2]*Graduate School of Engineering, Nagoya Institute of Technology, Nagoya 466-8555, Japan*

[3]*UVSOR Facility, Institute for Molecular Science, Okazaki 444-8585, Japan*

Heusler-type $Fe_2VAl$ and its related alloys have attracted much attention because of the enhancement of its thermoelectric power $S$ by partial substitution of the forth element $M$ [1]. Universal dependence of $S$ is found on the partial substitution, which can be qualitatively explained by a rigid-band-model. However, it is also noticed that $S$ depends on a substituted element $M$ even in the same group, as shown in Fig. 1 [2]. To develop new thermoelectric materials, it is important to understand the origin of the dependence of their thermoelectric properties on the substitution. In this report, we will show the results of the 3*p*-3*d* resonance photoemission measurement of $Fe_{2-y}M_yVAl$ ($M$ = Co, Rh, and Ir) to clarify the change in their electronic structure on the substitution.

Photoemission spectra of polycrystalline samples of $Fe_{2-y}M_yVAl$ were recorded under ~2 x $10^{-8}$ Pa at 20 K for clean surfaces prepared by *in situ* fracturing.

Figure 1 summaries valence-band spectra of $Fe_{1.9}M_{0.1}VAl$ recorded at the excitation photon energy $h\nu$ of 52 and 37 eV just below the Fe and V $M_{2,3}$ thresholds, where the Fe and V 3*d* photoemissions are suppressed due to so-called anti-resonance effect, respectively. Thus the spectra at $h\nu$ = 52 eV may represent the density of states (DOS) other than the Fe 3*d* states, *i.e.* the V and *M d* states, while the spectra at $h\nu$ = 37 eV show the Fe and *M d* DOS. In all the spectra, there are features recognized at the binding energy of $E_B$ ~ 0.4, 0.8, 1.5, and 3 eV. As seen in the spectra at $h\nu$ = 52 eV, the *d* DOS of V and substituted *M*, is almost the same for all the studied alloys. At $h\nu$ = 37 eV, the 0.8-eV band for the Co substitution becomes prominent, while the spectra for the Rh and Ir substitution are similar to each other. Small band shift towards the high binding energy side as a whole is also noticed for the Ir substitution.

Observed similarity is ascribed to the common band formation with the substituted *M d* states incorporated into the main Fe-V 3*d* band. According to Harisson [3], the characteristic radius $r_d$ of Co 3*d* states compared with the Fe 3*d* ones is slightly reduced but those of the Rh 4*d* and Ir 5*d* ones are much increased. Thus the interaction of the Rh and Ir *d* states with the Fe 3*d* ones, proportional to $r_d^3$, is expected to be larger than the Co-Fe interaction. On the other hand, the average *d* state energy $\varepsilon_d$ of Co is low and those of Rh and Ir are high, compared with that of Fe. Therefore the Fe 3*d* states are expected to be pushed towards the high and low binding energy side for the Ir and Co substitutions, respectively; the large interaction of Ir with Fe suggests larger shift than that of Co. This seems consistent with the present results.

Further study of the dependence on the substitution is now in progress and will be reported elsewhere.

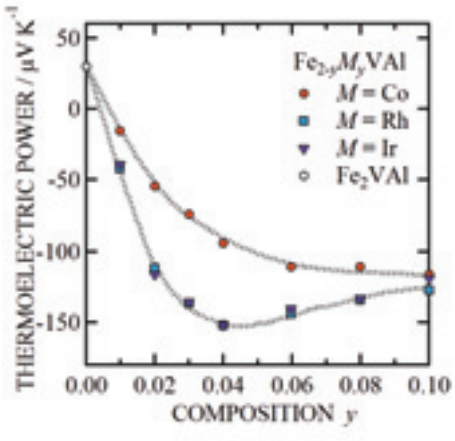


Fig. 1. Thermoelectric power of Heusler-type alloys $Fe_{2-y}M_yVAl$ ($M$ = Co, Rh, and Ir).

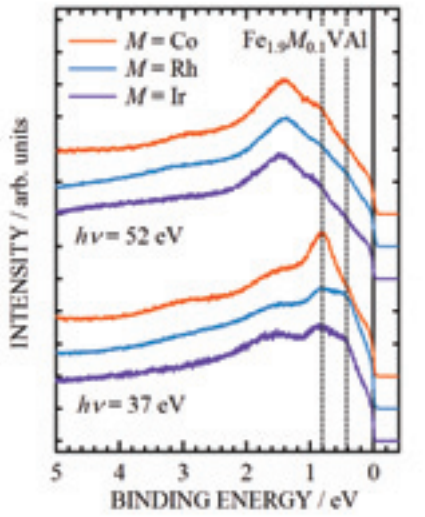


Fig. 2. Valence-band photoemission spectra of Heusler-type alloys $Fe_{1.9}M_{0.1}VAl$ ($M$ = Co, Rh, and Ir)

[1] Y. Nishino, "The Science of Complex Alloy Phases," (TMS, Warrendale, 2005) 325.

[2] T. Sugiura and Y. Nishino, J. Jpn. Inst. Metals **73** (2009) 846.

[3] W. A. Harisson, "Electronic Structure and the Properties of Solids," (Dover Publications Inc., New York, 1989).

BL5U

# A Photon Energy-Dependent Angle-Resolved Photoemission Study of $CaCu_3Ti_4O_{12}$

H. J. Im[1], T. Sakurada[1], M. Tsunekawa[2], M. Toita[1], T. Watanabe[1], K. Takegahara[1], H. Miyazaki[3] and S. Kimura[3,4]

[1]*Department of Advanced Physics, Hirosaki Univerisy, Hirosaki 036-8561, Japan*
[2]*Faculty of Education, Shiga University, Shiga 522-8522, Japan*
[3]*UVSOR Facility, Institute for Molecular Science, Okazaki 444-8585, Japan*
[4]*School of Physical Sciences, The Graduate University for Advanced Studies, Okazaki 444-8585, Japan*

Recently, the discovery of the extremely high dielectric constant (as high as $10^4$-$10^5$) of A-site perovskite $CaCu_3Ti_4O_{12}$ (CCTO) over a wide range of temperature from 100 to 500 K has generated considerable attention because of the expectation of developing a high-efficient and small capacitor [1, 2]. However, its electronic structures are not still clear due to the absence of observation of band dispersion. Furthermore, discrepancy between the results of electrical transport measurements and that of band calculation has stressed an importance of the observation of band dispersion; while CCTO has a metallic phase in LDA band calculation, the electrical resistivity measurements exhibit an insulator phase. Here, we clearly observed the band dispersions in valence band regime and found the high symmetry points (Γ and H), using photon energy (*hv*)-dependent angle-resolved photoemission spectroscopy (ARPES).

High-quality CCTO single crystal was prepared by TSFZ method. ARPES experiments were performed at the beamline BL5U. The range of photon energies is from 54 eV to 93 eV. The clean surface was prepared in the (100) plane by cleaving *in situ*. Measurements were carried out at room temperature ($T$ = 300 K) in a vacuum better than $2\times10^{-8}$ Pa. A wide angle acceptable MBS analyzer is used with energy resolution of 50 meV at $hv$ = 60 eV.

Figure 1 (a) shows the energy distribution curves (EDCs) of CCTO in the valence-band region along Δ-direction. With increasing *hv*, ARPES spectra trace the blue dashed arrow in the Brillouin zone of body-centered cubic structure depicted as in Fig. 1 (b). Valence bands can be divided into three regions, 1 - 2.5 eV, 2.5 - 5 eV, and 5 - 8 eV. The bands in the regions of 2.5 - 5 eV and 5 - 8 eV relatively highly disperse with intense features, while the bands in the region of 1 - 2.5 eV are not well distinguished due to weak intensity and broad band width. In the region of 1- 2.5 eV, we observe the intensity variation of the small shoulder as a function of *hv*, reflecting the band dispersion. The shoulder becomes prominent closing $hv$ = 60 eV. This suggests that $hv$ = 60 eV is a symmetry point. In the region of 2.5 - 5 eV, there are two kinds of bands. One disperses from 2.9 to 3.5 eV with a top at $hv$ = 90 eV, while the other shows very small dispersion around 3.9 eV, reflecting the localized character. In the region of 5 - 8 eV, bands are well split with top around 5.5 eV and bottom around 7.4 eV around $hv$ = 90 eV. These indicate that both $hv$ = 60 and 90 eV correspond to symmetry point. According to the free electron final state model, the inner potential is estimated to be 16 eV and the symmetry points are designated as shown in Fig. 1 (a): the EDC at $hv$ = 90 eV corresponds to Γ-point and that of $hv$ = 60 eV to H-point. Finally, we find the negligible intensity at the Fermi level ($E_F$), which directly explains why CCTO shows the insulator phase.

We performed *hv*-dependent ARPES measurements on A-site perovskite CCTO, which shows extremely high-dielectric constant and has an insulator phase in contrast to band calculation results. We observed the clear band dispersions and the negligible spectral weight at $E_F$ in good agreement with the electrical resistivity measurements.

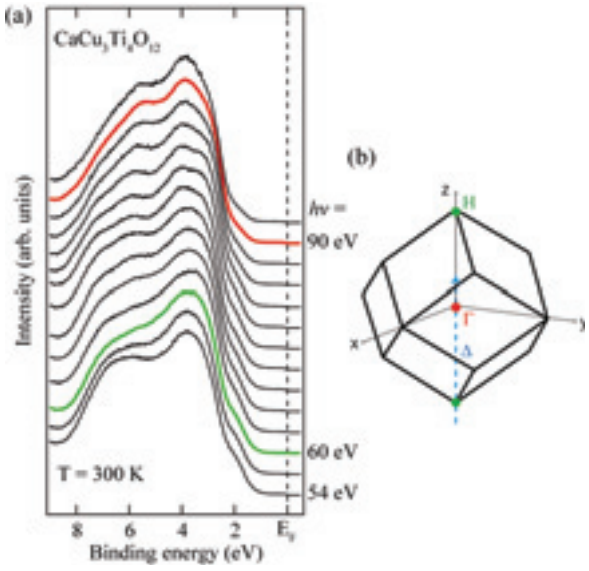


Fig. 1. (a) The EDCs along Δ-direction obtained by ARPES measurements at photon energies between $hv$ = 54 and 93 eV in normal emission. (b) The Brillouin zone and the momentum spaces (blue dashed arrow) measured in experiments.

[1] M. A. Subramanian *et al.*, J. Solid State Chem. **151** (2000) 323.
[2] Y. Zhu *et al.*, Phys. Rev. Lett. **99** (2007) 037602.

BL5U

# Angle-Resolved Photoemission Study on $GdTe_2$

R. Niwa[1], S. Hirate[2], T. Ito[1,4], T. Hajiri[1], H. Miyazaki[3], B. H. Min[6], S. Kimura[3,5] and Y. S. Kwon[6]

[1]*Graduate School of Engineering, Nagoya University, Nagoya 464-8603, Japan*
[2]*School of Engineering, Nagoya University, Nagoya 464-8603, Japan*
[3]*UVSOR Facility, Institute for Molecular Science, Okazaki 444-8585, Japan*
[4]*Nagoya University Synchrotron radiation Research Center, Nagoya University, Nagoya 464-8603, Japan*
[5]*School of Physical Sciences, The Graduate University for Advanced Studies (SOKENDAI), Okazaki 444-8585, Japan*
[6]*Department of Physics, Sungkyukwan University, Suwon 440-749, Korea*

Rare-earth ditellurides ($RTe_2$; $R$ = rare earth) have attracted much attention because of their anomalous physical properties due to their two dimensionality, especially the charge density wave (CDW) transition [1]. However, there are not many reports of CDW formation from the electronic structure viewpoint except for $LaTe_2$ and $CeTe_2$ [2].

In this study, we have performed angle-resolved photoemission spectroscopy (ARPES) on single -crystalline $GdTe_2$ [3] to clarify the CDW formation and its relation to the anomalous properties.

Figure 1 shows the Fermi surface (FS) of $GdTe_2$ at the temperature $T$ of 10 K obtained by the intensity plot of the ARPES spectra in the binding energy region of $E_F \pm 20$ meV with the incident photon with the energy of 63 eV. The perfectly symmetric FS images are consistent with the bulk Brillouin zone. This result implies that the observed electronic structure corresponds to the bulk electronic structure. From band structure calculations on $RTe_2$ [2], FSs dominate with Te $5p_x$ and $5p_y$ characters.

Figure 2 (a) shows the ARPES image near $E_F$ along the ΓX high-symmetry line. Two symmetric bands with respect to the Γ point are observed. These bands are attributed to a hole pocket at around the Γ point and an electron pocket at around the X point. The intensity of these bands are suppressed at the binding energy ($E_B$) of 0.25 eV. Similar suppression was observed in the whole Brillian zone. To check the suppression of intensity at $E_B = 0.25$ eV in detail, the energy distribution curves are plotted in Fig. 2 (b). This figure clearly indicates that the conduction band is folded at around $E_B = 0.25$ eV and the gap opens in between $E_B = 0.1$ and 0.4 eV. The band folding as well as the energy gap is the evidence of the CDW formation.

[1] J. Chung *et al.*, J. Kor. Phys. Soc. **38** (2001) 744.
[2] K. Y. Shin *et al.*, Phys. Rev. B **72** (2005) 085132.
[3] Y. S. Kwon and B. H. Min, Physica B **281&282** (2000) 120.

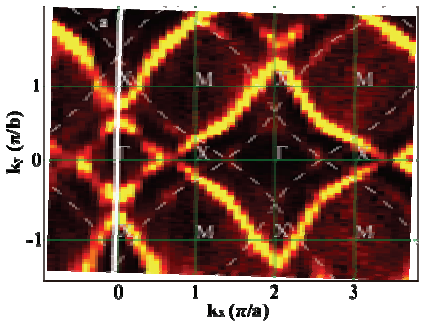


Fig. 1. The intensity map of the ARPES spectra of $GdTe_2$ in the binding energy width of $E_F \pm 20$ meV plotted in the ΓXM plane of the Brillouin zone. The ARPES spectra were taken at $T = 10$ K using $hv = 63$ eV photons. The plot can be regarded as a Fermi surface.

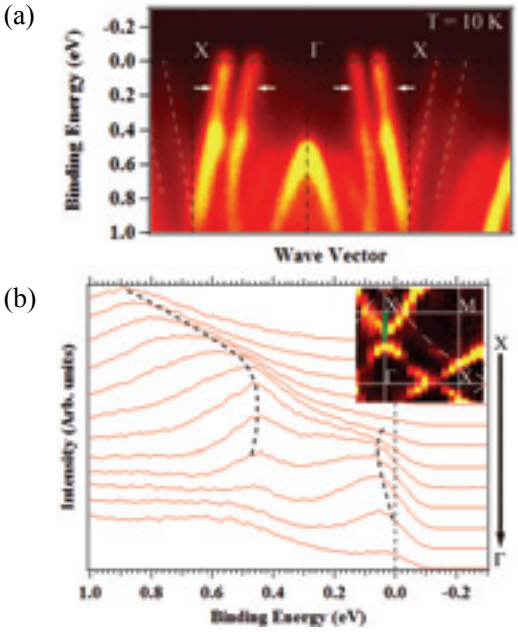


Fig. 2. (a) ARPES image along the ΓX symmetry line. White dashed lines are guides for eyes. (b) ARPES spectra near $E_F$ of $GdTe_2$ enlarged around FS crossing point of the electron pocket at the X point (green line in inset). These data were taken at $T = 10$ K using $hv = 63$ eV photons.

BL6B

# Terahertz Spectroscopy of Copper Ion Conducting Glasses

T. Awano

*Department of Electronic Engineering, Tohoku Gakuin University, Tagajo 985-8537, Japan*

An optical absorption band by a collective motion of mobile ions may appear in terahertz region, in which motion of mobile ions changes from translation in microwave region to vibration motion in far-infrared region. I had investigated far-infrared and millimeter wave spectra of some silver or copper ion conductors to study the dynamics of mobile ions. In $AM_4X_5$ (A=alkali metal; M=Ag or Cu; X=halogen) crystal, a structure by "ionic plasmon" was observed in the spectral region below 10 $cm^{-1}$ in silver ion conductors or 30 $cm^{-1}$ in copper ion conductors in energy loss function spectra at temperatures of superionic conducting phase [1].

Such collective motion may be one reason of the high ionic conductivity of superionic conducting glasses even at low temperature. I had investigated whether such "ionic plasmon" exists in the non-periodic structure in glass of various frameworks. The $AgI$-$Ag_2MoO_4$ glass has no network structure in contrast with the $AgI$-$AgPO_3$. The alkylammonium ions (TMA, TEA) disperse randomly into AgI in organic-inorganic glasses.

In this study, I have investigated on copper ion conducting glasses of $CuI$-$CuPO_3$, $CuI$-$Cu_2MoO_4$ and TMAI-TEAI-CuI glasses to compare ionic motion with silver conducting glasses.

Figure 1 shows absorption spectra of $CuI$-$CuPO_3$, $CuI$-$Cu_2MoO_4$ and TMAI-TEAI-CuI glasses obtained from reflectivity spectra by K-K analysis. They are put in order of their CuI-contents. There observed two broad absorption bands around 130, 60, 30 $cm^{-1}$ and at low energy tail. These absorption bands were observed in silver conducting glasses, however, peak positions are slightly shifted toward high energy side in copper conducting glasses. This seems to be due to the difference of mass of conduction ion. Expected frequency ratio of silver and copper motion is 1.3 and is in good agreement with observed ones. This means that these bands are due to motions of conducting ion.

Figure 2 shows absorption spectra of silver ion conducting $AgI$-$Ag_2O$-$V_2O_5$ glasses for comparison. This glass has dispersive structure as the $AgI$-$Ag_2MoO_4$ glass, therefore is able to contain much AgI. Peak positions of broad absorption bands are 110 and 20 $cm^{-1}$. These positions are the same as those in other silver conducting glasses [2].

[1] T. Awano, Infrared Phys. and Tech. **51** (2008) 458.
[2] T. Awano and T. Takahashi, J. Phys. Soc. Jpn. **79** Suppl. A (2010) 118.

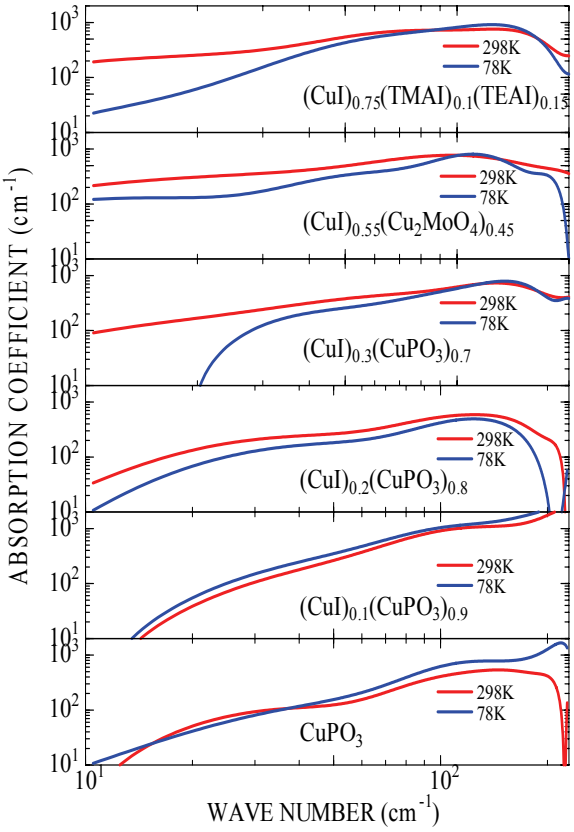


Fig. 1. Absorption spectra of CuI-containing superionic conducting glasses.

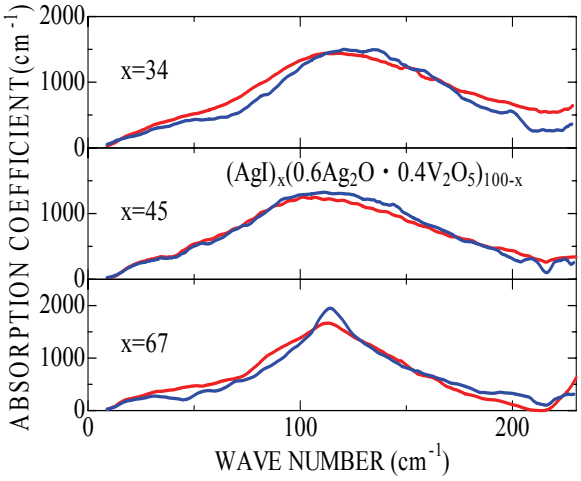


Fig. 2. Absorption spectra of AgI-containing superionic conducting glasses.

BL6B

# Pressure-Dependent Reflectivity Spectra of α-(BEDT-TTF)$_2$I$_3$ in the THz Region

T. Iizuka[1], T. Mori[2], K. Yakushi[1,3] and S. Kimura[1,2]

[1]*School of Physical Sciences, The Graduate University for Advanced Studies (SOKENDAI), Okazaki 444-8585, Japan*

[2]*UVSOR Facility, Institute for Molecular Science, Okazaki 444-8585, Japan*

[3]*Institute for Molecular Science, Okazaki 444-8585, Japan*

## Introduction

Recently, a quasi-two-dimensional organic conductor, α-(BEDT-TTF)$_2$I$_3$ [BEDT-TTF = bis(ethylenedithio)tetrathiafulvalene, here after BEDT-TTF is abbreviated as ET] is attracting attention because of its rich physical properties, e.g., superconductivity under uniaxial pressure along the *a*-axis and a zero gap state, namely "Dirac-cone" as observed in graphite [1]. α-(ET)$_2$I$_3$ shows metal-to-insulator (M-I) transition on cooling due to charge ordering ($T_{CO}$ = 135 K), at ambient pressure. $T_{CO}$ decreases with applying pressure, and then disappears at around 2.0 GPa. Previously reported temperature-dependent hall coefficient and electrical resistivity data imply that the carrier density and mobility compensate each other above 1.9 GPa [2]. The anomalous carrier property is discussed to originate from the Dirac-cone-type conduction band [3]. However, there has been no direct observation of the electronic structure yet. In this study, the polarized optical reflectivity spectrum $R(\omega)$ of α-(ET)$_2$I$_3$ was measured under pressures to investigate the electronic structure.

## Experimental

Single crystals of α-(ET)$_2$I$_3$ were grown by an electrochemical oxidation method. Polarized $R(\omega)$ of α-(ET)$_2$I$_3$ along the *a*-axis was measured in the terahertz (THz) region of 70 - 450 cm$^{-1}$ (2.1 - 13.6 THz), from the insulator to metallic phases by applying pressure from 0.3 to 2.9 GPa at the temperature of 8 K. The measurement was performed at the THz micro-spectroscopy end station of BL6B at UVSOR-II. A diamond anvil cell (DAC) was employed to produce high pressure, with a pressure medium of Apiezon® N. The pressure was calibrated by a ruby fluorescence method.

Because of the low signal intensity in the insulator phase, the accumulation was done in form of interferogram. Spectra were calculated from the Fourier transformation of the averaged interferograms.

## Results and Discussion

Obtained $R(\omega)$ of α-(ET)$_2$I$_3$ at $T$ = 8 K at pressures from 0.3 to 2.9 GPa are shown in Fig. 1. $R(\omega)$ at ambient pressure after the correction of using diamond window (reflective index $n$ = 2.4) in DAC is shown at the bottom of the figure [4].

TO-Phonon peaks at around 123 cm$^{-1}$, which mainly appear in the polarization along the *a*-axis, correspond to the antisymmetric stretching mode of $I_3$ [4]. The peaks do not shift below the M-I transition pressure of 2.0 GPa. On the other hand, phonon peaks at around 400 cm$^{-1}$ shift to the lower wavenumber side with elevating pressure. The latter peak comes from the breathing mode of ET molecules which can couple to carriers [4]. In addition, the base line of the spectrum increases with applying pressure due to the appearance of carriers. Even in the metallic phase above 2.0 GPa, the spectra have no Drude response, but the $R(\omega)$ intensity increases with increasing the wavenumber. The Drude response seems to appear in the lower energy region. This result is consistent with Dirac-cone picture which has low carrier density due to the unique electronic structure of Fermi "point", not a surface, in the Fermi level [3].

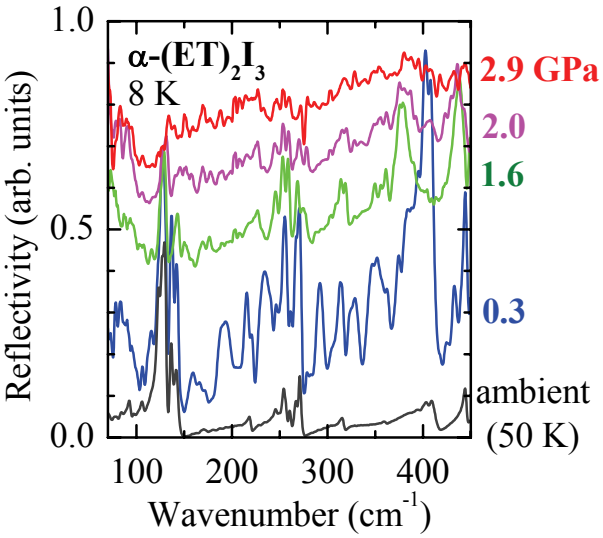


Fig. 1. Pressure-dependent reflectivity spectra [$R(\omega, P)$] of α-(ET)$_2$I$_3$ at the temperature of 8 K with polarization along the *a*-axis. Black line is the simulated reflectivity spectrum at ambient pressure in the case of a diamond window of DAC [4].

[1] A. B. Kuzmenko *et al.*, Phys. Rev. Lett. **100** (2008) 117401.
[2] N. Tajima *et al.*, J. Phys. Soc. Jpn. **69** (2000) 543.
[3] S. Katayama *et al.*, J. Phys. Soc. Jpn. **75** (2006) 054705.
[4] Y. Yue *et al.*, Phys. Rev. B **82** (2010) 075134.

BL6B

# LO-Phonon Plasmon Coupled Mode of ZnO

T. Inushima[1], Y. Ota[1] and K. Fukui[2]
[1]*Department of Electronics, Tokai University, Hiratsuka 259-1292, Japan*
[2]*Department of Electrical and Electronics Eng., University of Fukui, Fukui 910-8507, Japan*

There are several similarities in the electronic structures between InN and ZnO; it is predicted from the first principle calculation that whenever there is a defect, it produces electrons in the conduction band [1]; It is also predicted that neither the phonon structure nor the band structure can be obtained without taking into account the d electrons as valence electrons. So anomaly of the plasmon-longitudinal optical (LO) phonon coupled mode is a common subject to be investigated [2]. In this experiment, we measured the plasmon-LO phonon coupled mode of ZnO as a function of the electron density.

Using BL6B and a MCT detector we measured the reflectivity spectra of c-plane ZnO at a nearly normal incident configuration. Figure 1 shows the electron density dependence of the reflectivity spectra of bulk ZnO samples which were grown by hydrothermal method. The samples contain Li, which is considered to produce electrons as residual carriers in the conduction band. In this experimental configuration, only $E_1$ optical phonon is observed as a Reststrahren band (TO at 409 $cm^{-1}$ and LO at 587 $cm^{-1}$). The inset shows that the LO-phonon shoulder melts according to the increase of the electron density, and that linear plasmon-LO phonon coupling (Frölich interaction) is not observed. Another contribution of the electron is the decrease of reflectivity in the energy region higher than 1100 $cm^{-1}$. There is a cutoff of the second order phonon absorption at 1100 $cm^{-1}$. Then this decrease of the reflectivity is related to the increase of the impurities or defects in the sample.

Usually Germanium and Silicon are non-polar materials and the optical phonons at $k$=0 are not infrared active. Consequently they do not split at $k$=0 into LO and TO components, and there is no LO-phonon plasmon coupled mode. In these non-polar semiconductors the interaction between free carriers and phonons is non-linear and optical phonons are observed as a result of Fano interference. When interference exists, the LO phonon shows asymmetric broadening at the initial position. On the other hand, in polar semiconductors like InN, LO-phonon-plasmon interaction is so strong that only plasmon-LO phonon coupled modes are observed.

The results shown in Fig. 1 indicate that the LO phonons of ZnO do not couple with the free carriers linearly, but they show instead Fano interference.

From the first principle calculation ZnO has a spontaneous polarization of 0.05 $C/m^2$, which is comparable to that of the representative polar semiconductor AlN. Hence the absence of Frölich interaction in ZnO should be explained by taking into account the cause of the residual carriers in the conduction band.

In conclusion, polar semiconductor ZnO does not have plasmon-LO phonon coupled mode. To make clear this absence, reflectivity measurements in the far-infrared region are necessary, which will be done in the near future.

[1] Chris G. Van der Walle and J. Newgebauer, Nature **423** (2003) 626.
[2] T. Inushima, M. Higashiwaki and T. Matsui, Phys. Rev. B **68** (2003) 235204.

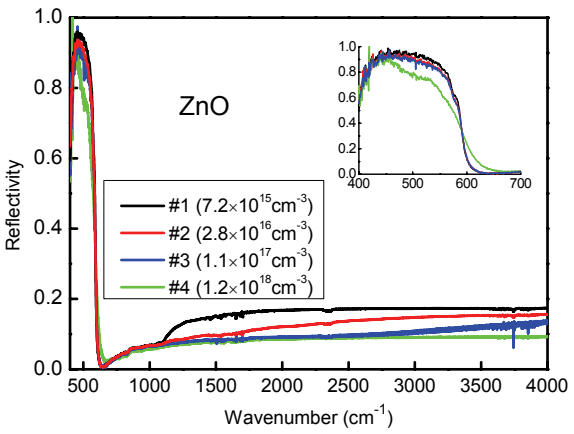


Fig. 1. Electron density dependence of the reflectivity spectra of bulk ZnO grown by a hydrothermal method. The incident light is normal to the a-b plane. Inset is the detail of the $E_1$ phonon Reststrahren band of ZnO.

BL6B

# Observation of Electronic States on Solids Utilizing FIR Synchrotron Radiation

A. Irizawa[1], T. Iizuka[2] and S. Kimura[2,3]

[1]*The Institute of Science and Industrial Research, Osaka University, Ibaraki 567-0047, Japan*

[2]*School of Physical Sciences, The Graduate University for Advanced Studies (SOKENDAI), Okazaki 444-8585, Japan*

[3]*UVSOR Facility, Institute for Molecular Science, Okazaki 444-8585, Japan*

## Introduction

The optical study is one of the most powerful techniques for the investigation of electronic states on solids. There can be obtained the great deal of information about the electronic band structure, the symmetry of crystal structure, and the dielectric property. In the respect of experimental affinity, the optical study is extremely compatible with the multiple conditions such as low temperature, high magnetic field, and high pressure. In the case of strongly correlated electron systems, it is well known that the temperature is one of the decisive factors for the electronic state. The considerable types of phase transition are induced by the change of the temperature. Particularly, the multiferroic compounds can be controlled of its physical properties mutually by the external fields such as magnetic, electronic, and elastic ones. The other particular condition, the pressure will directly affect the electron-electron interactions through the change of lattice constants. The beamline BL6B in UVSOR is adjusted for the investigations at low temperature and high pressure in the extremely low-energy region of IR-THz. There equips two type interferometers of both Michelson and Martin-Puplett type. In this report, we have performed the optical reflectivity measurements in the longest wavelength region for the newly synthesized compound having a spinel-related structure.

## Experimental

The selected experimental components are the Martin-Puplett type interferometer and the Si-bolometer detector with the liquid-He flow type cryostat for controlling the temperature from 300 K down to 13 K. The reflectivity was obtained from the ratio of optical reflections between the sample and Au as a standard with mirrored surfaces. They were installed on the sample holder and were measured through the tapered hole of 4 mm in diameter.

## Results and Discussion

The reflectivities are obtained in the energy range between 20 and 230 $cm^{-1}$ as shown in Fig. 1. Here we can confirm the gradual change from the metallic spectrum at 300 K to the insulating ones with decreasing temperature. The Drude response toward 1 clearly decreases at low temperatures. More than 3 phonons are uprising in the insulating state except the intrinsic noise coming from the Fourier-transform (FT) interferometer at around 40 $cm^{-1}$. The obtained spectra are well connected to the higher-energy spectra measured at the laboratory using the conventional light source, i.e., black body. The comprehensive reflectivity including this result will develop the reliable optical constants through the Kramers-Kronig (KK) transform.

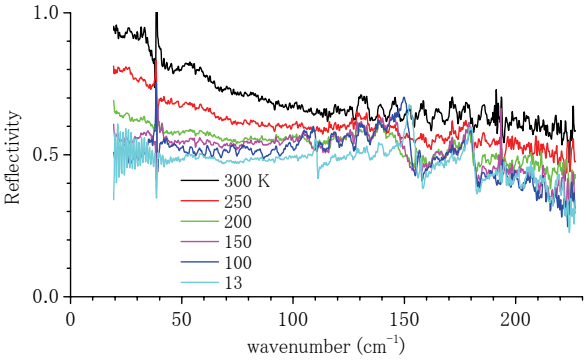


Fig. 1. Temperature change of the reflectivity at the FIR-THz region.

BL7U

# Polarization-Dependent Angle-Resolved Photoemission Study on LiFeAs

T. Hajiri[1], R. Niwa[1], T. Ito[1,2], M. Matsunami[3,4], Y. J. Song[5], S. Kimura[3,4] and Y. S. Kwon[5]

[1]*Graduate School of Engineering, Nagoya University, Nagoya 464-8603, Japan*

[2]*Nagoya University Synchrotron radiation Research Center, Nagoya University, Nagoya 464-8603, Japan*

[3]*UVSOR Facility, Institute for Molecular Science, Okazaki 444-8585, Japan*

[4]*School of Physical Sciences, The Graduate University for Advanced Studies (SOKENDAI), Okazaki 444-8585, Japan*

[5]*Department of Physics, Sungkyunkwan University, Suwon 440-749, Korea*

Iron pnictide superconductor discovered recently [1]. Although they have been intensively studied from both experiment and theory, the mechanism of its anomalous superconductivity has not been revealed yet. So far, the importance of the orbital characters of Fermi surfaces for the nesting condition has been reported [2]. However, there are few reports about the nesting properties on the three-dimensional electronic structure [3].

We have performed angle-resolved photoemission spectroscopy (ARPES) on LiFeAs ($T_c$ = 18 K), to elucidate the three-dimensional electronic structure, especially Fermi surfaces and the orbital characters, by using S and P polarized photons at UVSOR-II BL7U as shown in Fig. 1 (a).

Figure 1 (b) shows the photon-energy-dependent ARPES spectra at $k$ = 0 Å$^{-1}$ of LiFeAs measured at $T$ = 12 K (SC state) with the P polarization. The ARPES peak disperses from 0.4 eV (hν = 23 eV) to 0.3 eV (hν = 35 eV). The observed symmetry shows in good agreement with the π/c (ΓZ, see Fig. 1 (c)) period.

Figures 2 (a) and (b) show the polarization -dependent ARPES image near the Γ and Z points, respectively. Red and green color maps are ARPES images for the S and P polarized photons, respectively. In Figure 2, the three (two) hole-pockets near the Γ (Z) point show the clear polarization dependence between S and P polarizations. According to the dipole selection rules [4], ARPES spectra with S polarization are dominated by $d_{xy}$ and $d_{yz}$ orbitals (with odd symmetries), while P polarization with $d_{xz}$, $d_{x^2-y^2}$ and $d_{z^2}$ (with even symmetries). It should be noted that the $d_{xz}$ orbital cross section is larger than that of $d_{x^2-y^2}$ at this photon energy [5]. Thus we conclude the orbital character of each FS as follows; (1) $d_{yz}$ for the middle hole-pocket at the Γ point and for inner hole-pocket at the Z point, (2) $d_{x^2-y^2}$ for the outer hole-pocket at the Γ and Z point, and (3) $d_{xz}$ for the inner hole-pocket at Γ point, respectively. The above characterizations are in good agreement with the band calculation [6].

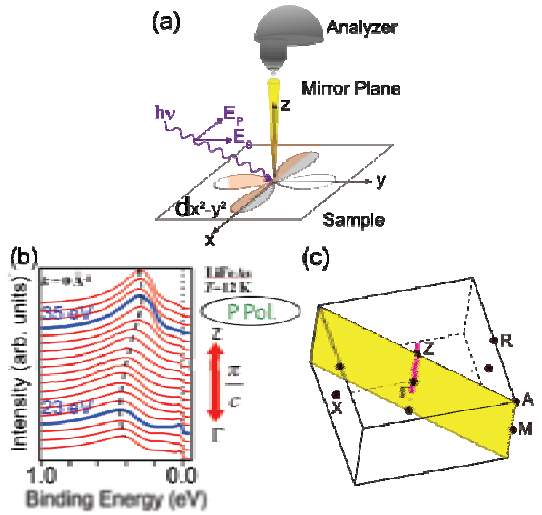


Fig. 1. (a) Experimental configuration of present ARPES. (b) Photon-energy-dependent ARPES spectra at $k$ = 0 Å$^{-1}$ of LiFeAs at $T$ = 12 K with the P polarization. (c) Brillouin zone of LiFeAs. The red line corresponds to the measured line in (b) in the ΓMAZ plane (yellow area).

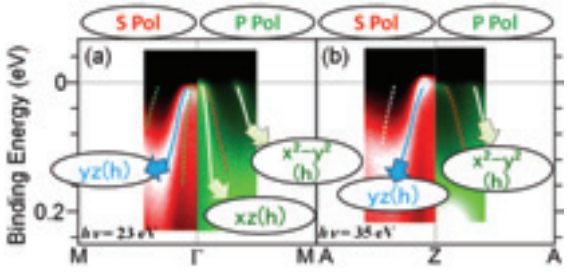


Fig. 2. ARPES image near the Γ (a) and Z (b) points of LiFeAs at $T$ = 12 K measured with the S (red image) and P (green image) polarizations.

[1] Y. Kamihara *et al.*, J. Am. Chem. Soc. **130** (2008) 3296.
[2] K. Kuroki *et al.*, Phys. Rev. B **79** 224511 (2009).
[3] T. Yoshida *et al.*, Phys. Rev. Lett. **106** (2011) 117001.
[4] A. Damascelli, Physica Scripta. **T109** (2004) 61.
[5] B. Mansart *et al.*, Phys. Rev. B **83** (2011) 064516.
[6] S.V. Borisenko *et al.*, Phys. Rev. Lett. **105** 067002 (2010).

BL7U

# Three-Dimensional ARPES Study on $FeSb_2$

S. Imada[1], K. Terashima[1], A. Yamasaki[2], K. Mima[1],Y. Miyata[1], R. Yamaguchi[1], Y. Tachimori[1], Y. Yamanoi[1], H. Eto[1], Y. Matsui[2], J. Yamaguchi[3], S. Komori[3], A. Sekiyama[3], S. Suga[3] and H. Nakamura[4]

[1]*Faculty of Sci. and Eng., Ritsumeikan University, Shiga 525-8577, Japan*
[2]*Faculty of Sci. and Eng., Konan University, Kobe 658-8501, Japan*
[3]*Grad. School of Eng. and Sci., Osaka University, Osaka 560-8531, Japan*
[4]*Grad. School of Eng., Kyoto University, Kyoto 606-8501, Japan*

$FeSb_2$ shows a metal-insulator crossover; it is metallic around room temperature, while it is insulating at low temperatures with an upturn of the resistivity curve at ~50 K. A number of experimental reports have indicated the existence of the energy gap at low temperatures [1-3], while the mechanism for the formation of the energy gap has not been settled yet. So far, mainly two scenarios have been proposed, one is that $FeSb_2$ is a Kondo insulator [2], and the other is that $FeSb_2$ is a narrow-gap semiconductor [1, 3].

In our previous study on $FeSb_2$ at UVSOR [4], we have measured temperature dependence of the density of states (DOS) near $E_F$. As we reduce the temperature, the DOS suppression is observed, but finite intensity in the vicinity of $E_F$ remains even at 15 K where the resistivity shows insulating behavior. We also find a free-electron like band crossing $E_F$ at 15 K, indicative of the surface state. Thus it is important to separate the surface contribution from photoemission spectra to discuss bulk property and its mechanism.

In the present study, we have performed angle-resolved photoemission (ARPES) on $FeSb_2$ to reveal the mechanism of the crossover by directly observing the temperature dependence of the energy gap. Since the band calculation predicts three-dimensional band structure and the existence of a couple of small Fermi surfaces [5, 6], we measured $h\nu$-dependence of the normal emission spectra to determine inner potential of the sample.

A single crystal of $FeSb_2$ has been synthesized by Sb-flux method. High-resolution ARPES study has been performed at BL7U in the UVSOR facility. Energy resolution was set at ~15 meV. We have obtained a clean surface of the sample by fracturing in an ultrahigh-vacuum of ~$5\times10^{-9}$ Pa.

Figure 1 (a) shows the normal emission spectra using photon energy from 13 to 28 eV, where each $h\nu$ corresponds to different $k$ points along Γ-X axis. As in Fig. 1 (a), we have observed a number of dispersive bands of $FeSb_2$, such as Fe $3d_{3z^2-r^2}$ band [5] located at ~0.3 eV, Fe $3d_{x^2-y^2}$ band [5] at ~1 eV, and so on. In fig. 1 (b), the calculated bands [6] are tentatively superimposed on the plot of the second derivative of the normal emission spectra. From the comparison between our experimental results and calculated bands, we estimate that the spectra taken at $h\nu$~23 eV corresponds to Γ. The inner potential of $FeSb_2$ was calculated to be ~21 eV. With this inner potential, X point corresponds to $h\nu$~37 eV, and we find that BL7U can cover the whole Brillouin Zone of $FeSb_2$. Further ARPES study, clarifying (i) the bulk Fermi surfaces near the Zone edge and corner [5], (ii) the location of the surface bands, (iii) the temperature dependence of bulk bands, is necessary to elucidate the origin of the metal-insulator crossover in $FeSb_2$.

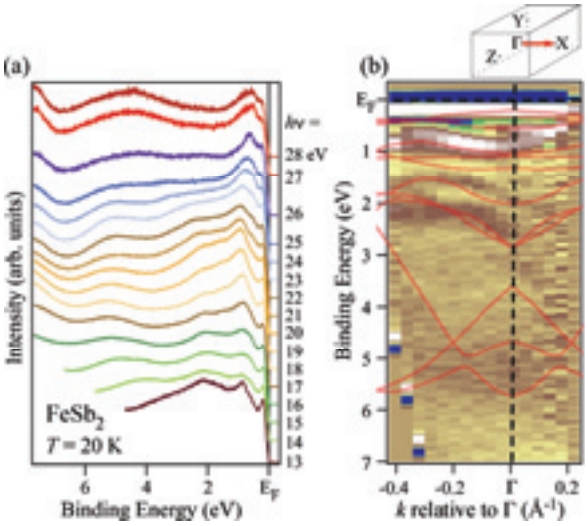


Fig. 1. (a) ARPES spectra derived by normal emission method using $h\nu$ = 13-28 eV at BL7U. (b) Plot of second derivative of (a). White and brown area corresponds to bands. Calculated bands [6] are shown as red lines. Inset shows Brillouin Zone of $FeSb_2$ and the measured $k$-direction (Red arrow).

[1] Z. Schlesinger *et al*., Phys. Rev. Lett. **71** (1993) 11.
[2] C. Petrovic *et al*., Phys. Rev. B **72** (2005) 045103.
[3] T. Koyama *et al*., Phys. Rev. B **76** (2007) 073203.
[4] S. Imada *et al*., UVSOR activity report **36** (2009) 106.
[5] A. V. Lukoyanov *et al*., Euro. Phys. J. **53** (2006) 205.
[6] J. M. Tomczak *et al*., Phys. Rev. B **82** (2010) 085104.

BL7U

# Angle-Resolved Photoemission Spectroscopy of $YbAl_2$

M. Matsunami[1,2], T. Hajiri[3], H. Miyazaki[1], M. Kosaka[4] and S. Kimura[1,2]

[1]*UVSOR Facility, Institute for Molecular Science, Okazaki 444-8585, Japan*

[2]*School of Physical Sciences, The Graduate University for Advanced Studies (SOKENDAI), Okazaki 444-8585, Japan*

[3]*Graduate School of Engineering, Nagoya University, Nagoya 464-8603, Japan*

[4]*Graduate School of Science and Engineering, Saitama University, Saitama 338-8570, Japan*

The heavy fermion or the valence fluctuation behavior in the strongly correlated *f* electron systems can be derived from the hybridization between conduction band and 4*f* state (*c-f* hybridization). Therefore, to directly probe the *c-f* hybridized electronic structures in the momentum space is important for understanding the heavy fermion physics. Angle-resolved photoemission spectroscopy (ARPES) is a powerful tool for this purpose. Recently, some ARPES results regarding the *c-f* hybridized electronic structure were reported [1-4]. These studies were performed on the basis of the surface Brillouin zone [1, 4] or by using the 4*d*-4*f* resonant process [2, 3]. However, ARPES for the *f* electron systems, which usually have three-dimensional electronic structure, should be done along the bulk Brillouin zone.

$YbAl_2$, which crystallizes in the cubic Laves $MgCu_2$ structure, is a prototypical valence fluctuation system. The Yb mean valence has been estimated to be ~ +2.2 by the resonant inelastic x-ray scattering experiment [5]. The electronic specific-heat coefficient as a measure of the electron-mass enhancement exhibits a slightly high value, $\gamma$~10-17 $mJ/K^2mol$ [6]. These characteristics suggest that a strong *c-f* hybridization effect can be realized in $YbAl_2$. Hence $YbAl_2$ is well-suited system for studying the *c-f* hybridized electronic structures including the *f* electron dispersion.

In this work, we have performed ARPES for $YbAl_2$. The single crystals of $YbAl_2$ were grown by the Lithium flux method [6]. The ARPES experiment was carried out at the undulator beamline BL7U "SAMRAI" in UVSOR-II [7]. The total energy resolution was set to ~10 meV and the measurement temperature was 12 K. The crystal orientation was determined by Laue x-ray diffraction prior to the ARPES measurements. The crystal was cleaved *in situ* at 12 K along the (111) plane.

Figure 1 (a) shows the bulk Brillouin zone of $YbAl_2$. The photon energy $h\nu$= 20 eV were chosen so as to obtain the electronic band dispersion in the Γ-K line as shown in Fig. 1 (b). The electron pocket centered at Γ point and the nearly flat bands at the binding energy of 0.15 eV are observed, which are attributed to Yb 5*d* conduction and Yb $4f_{7/2}$ bands, respectively. These states are strongly hybridized with each other, providing a fractional dispersion in Yb $4f_{7/2}$ bands.

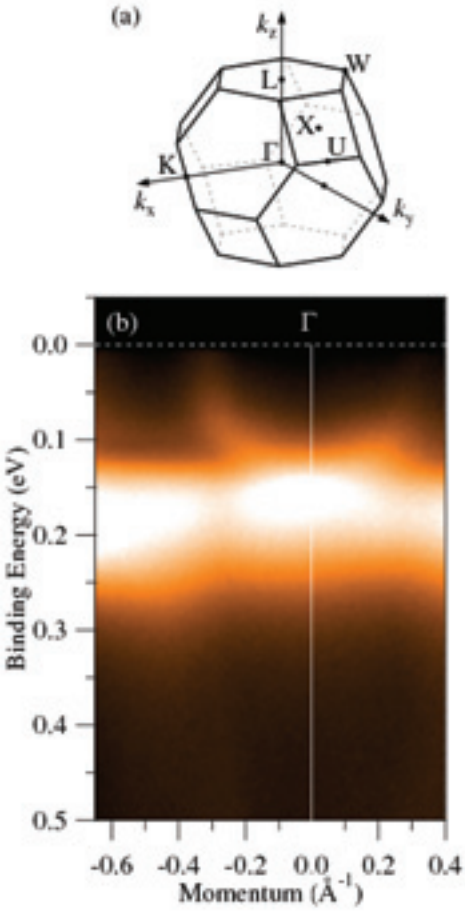


Fig. 1. The Brillouin zone (a) and the ARPES intensity map around Γ point at 12 K (b) of $YbAl_2$.

[1] S. Danzenbacher *et al*., Phys. Rev. Lett. **96** (2006) 106402.
[2] G. A. Wigger *et al*., Phys. Rev. Lett. **76** (2007) 035106.
[3] H. J. Im *et al*., Phys. Rev. Lett. **100** (2008) 176402.
[4] D. V. Vyalikh *et al*., Phys. Rev. Lett. **105** (2010) 237601.
[5] C. Dallera *et al*., Phys. Rev. B **68** (2003) 245114.
[6] H. Nowatari *et al*., J. Phys. Soc. Jpn. **76** (2007) Suppl. A, pp. 80.
[7] S. Kimura *et al*., Rev. Sci. Instrum. **81** (2010) 053104.

BL7U

# Temperature-Dependent Angle-Resolved Photoemission Spectra of $SmB_6$ (001)

H. Miyazaki[1], T. Hajiri[2], T. Ito[2] and S. Kimura[1,3]

[1]*UVSOR Facility, Institute for Molecular Science, Okazaki 444-8585, Japan*

[2]*Graduate School of Engineering, Nagoya University, Nagoya 464-8603, Japan*

[3]*School of Physical Sciences, The Graduate University for Advanced Studies, Okazaki 444-8585, Japan*

Rare-earth intermetallic compounds generally become metals with strong electron correlations. However, some compounds become semiconductors with very small energy gap at the Fermi level ($E_F$), namely "Kondo semiconductor" or "Kondo insulator" [1]. $SmB_6$ is one of Kondo semiconductors. The energy gap formation of $SmB_6$ has been debated for a long time because the origin of the energy gap has been unclear yet. To solve this problem, it is important to investigate the detailed electronic structure of $SmB_6$. Three-dimensional angle-resolved photoemission spectroscopy (3D-ARPES) using synchrotron radiation is the most powerful technique to determine the electronic band structure directly. Then we have performed 3D-ARPES to clarify the momentum-dependent electronic structure near $E_F$.

A $SmB_6$ (001) single crystal was cleaned by Ar+ ion sputtering and 1400 °C annealing cycles in the ultrahigh vacuum (UHV) chamber with a base pressure of ~ 2 × $10^{-8}$ Pa. Clean surface of $SmB_6$ with the 2 × 2 (001) patterns was confirmed by a low energy electron diffraction (LEED) method and no contamination, such as carbon, was checked by an Auger electron spectroscopy (AES). The 3D-ARPES measurements were performed at the beamline 7U of UVSOR-II. The total energy and momentum resolutions for the ARPES measurement were set to 13 meV and 0.006 $Å^{-1}$ at the Γ point ($h\nu$ = 26 eV) and 12 meV and 0.003 $Å^{-1}$ at the X point ($h\nu$ = 10.6 eV), respectively.

Figures 1 (a1) and (b1) show the temperature dependence of the energy distribution curves (EDCs) at the Γ and X points, respectively. The Fermi edge of the EDCs is broadened with elevating temperature due to the thermal excitations of electrons. With decreasing temperature, we observed broad and sharp peaks at around 20 meV at the Γ and X points, respectively, and small gap opening at both points. To clarify the temperature-dependent components near $E_F$, Figs. 1 (a2) and (b2) indicate density of states (DOS) derived from the EDCs derived by the Fermi-Dirac function evaluated from the gold at Γ and X points, respectively. DOS at $E_F$ gradually decreases with decreasing temperature at both the Γ and X points. However, only at the X point, a peak around 15 meV appears below 100 K and becomes larger on cooling. According to the temperature-dependent X-ray adsorption spectra (XAS) at the $L_{2,3}$-edge, the mean valence of Sm ions is dramatically changed from 2.57 at 120 K to 2.50 at 30 K [2]. The temperature dependence of the 15 meV peak at the X point is consistent with the XAS result, i.e., the 20 meV peak is strongly related to the change of the valence. According to the LDA band structure calculation, the hybridization between the Sm 5*d* and 4*f* states appears and the energy gap opens at the X point. Therefore the hybridization scenario is plausible for the semiconducting nature of $SmB_6$.

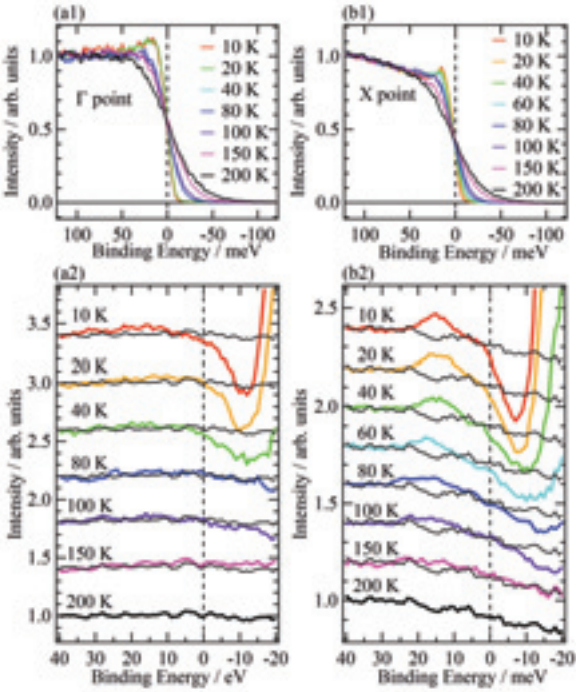


Fig. 1. Temperature dependence of the energy distribution curves (EDCs) and density of states (DOS) of SmB6 derived from the EDCs divided by the Fermi-Dirac function near the Γ point (a1, a2) and X point (b1, b2), respectively.

[1] G. Aeppli and Z. Fisk, Comment Condens. Matter Phys. **16** (1995) 1629.

[2] M. Mizumaki *et al.*, J. Phys.: Conf. Ser. **176** (2009) 012034.

BL7U

# High-Resolution Angle-Resolved Photoemission Study of an Iron Pnictide $CaFe_2P_2$: Observation of Strong $k_z$ Dispersion

K. Nakayama[1], T. Kawahara[1] P. Richard[2], K. Umezawa[1], T. Sato[1,3] and T. Takahashi[1,2]

[1]*Department of Physics, Tohoku University, Sendai 980-8578, Japan*

[2]*WPI Research Center, Advanced Institute for Materials Research, Tohoku University, Sendai 980-8577, Japan*

[3]*TRIP, Japan Science and Technology Agency (JST), Kawaguchi 332-0012, Japan*

The discovery of superconductivity in $LaFeAsO_{1-x}F_x$ below a transition temperature ($T_c$) of 26 K [1] has generated great interest. Owing to intensive researches, a lot of related compounds, which contain iron-pnictide (FeAs or FeP) layer, have been discovered. An important current issue is why physical properties show remarkable differences between the FeAs and FeP compounds despite an identical carrier number (Fe 3*d* electrons). For example, the highest $T_c$ is about one order of magnitude different (~56 K and ~7 K for FeAs and FeP compounds, respectively). It is also known that the non-doped FeAs compound exhibits an antiferromagnetic (AF) order accompanied by a structural phase transition, while the FeP compound does not show either magnetic or structural transition. To understand the origin of these differences in terms of electronic structure, angle-resolved photoemission spectroscopy (ARPES) is a powerful technique. Indeed, ARPES has revealed several essential features responsible for the superconductivity and AF order in the FeAs compounds, particularly in $AFe_2As_2$ ($A$ = Ca, Sr, and Ba) system, such as Fermi-surface topology, superconducting-gap symmetry, and band folding in the AF phase [2-5]. On the other hand, little is known about the electronic structure of the FeP compounds.

In this study, by utilizing the low energy and variable photon energy ($h\nu$) characters of the beamline BL7U, we have succeeded in directly observing three-dimensional bulk band dispersions in $CaFe_2P_2$, which does not show superconducting and AF transitions.

Figure 1 (a) shows ARPES spectral intensity plot along Γ(Z)-M(A) high-symmetry line measured with $h\nu$ = 23 eV. As denoted by black curves in Fig. 1 (a), we identify several highly dispersive bands such as a holelike α band and an electronlike γ band which cross Fermi level ($E_F$) at the Γ(Z) and M(A) points, respectively. To clarify the dimensionality of the electronic structure, we have performed systematic $h\nu$ dependence at the Γ(Z) point. As clearly seen from Fig. 1 (b), the holelike bands exhibit significant dispersions as a function of $h\nu$. For example, the α band is located at ~100 meV below $E_F$ for $h\nu$ = 15 eV, while it is above $E_F$ for $h\nu$ = 23 eV [Fig. 1 (a)], clearly indicating the presence of three-dimensional closed Fermi surface in $CaFe_2P_2$. This result is in sharp contrast to the previous observation of quasi-two-dimensional cylindrical Fermi surface in the normal state of $CaFe_2As_2$ [4]. The observed difference in the dimensionality of the electronic structure may be a key in understanding the differences between the FeAs and FeP compounds. It has been argued that the nesting between hole and electron Fermi surfaces plays an important role for the occurrence of the superconductivity and the AF order in iron pnictides. It is thus inferred that lower $T_c$ and the absence of the AF order in the FeP compound is caused by the deterioration of the nesting condition due to higher dimensionality, which may be associated with the shorter *c*-axis length compared to the FeAs compound.

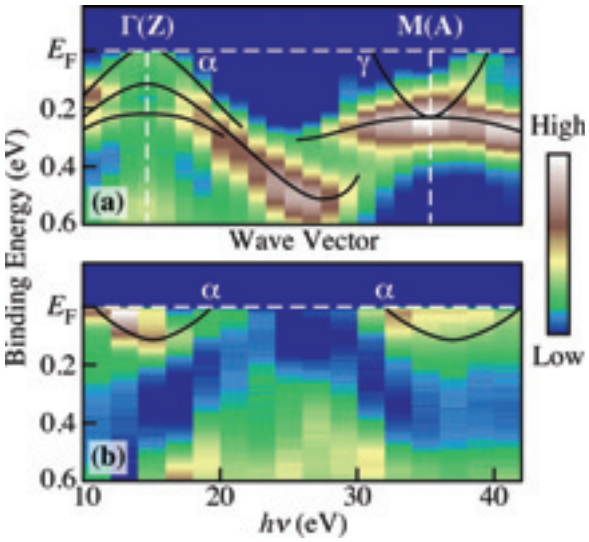


Fig. 1. (a) ARPES intensity of $CaFe_2P_2$ plotted as a function of wave vector and binding energy measured at 25 K with $h\nu$ = 23 eV. (b) $h\nu$ dependence of ARPES intensity at the Γ(Z) point. Black curves are guides for the eyes to trace the band dispersion.

[1] Y. Kamihara *et al.*, J. Am. Chem. Soc. **130** (2008) 3296.
[2] H. Ding *et al.*, Europhys. Lett. **83** (2008) 47001.
[3] K. Nakayama *et al.*, Europhys. Lett. **85** (2009) 67002.
[4] C. Liu *et al.*, Phys. Rev. Lett. **102** (2009) 167004.
[5] P. Richard *et al.*, Phys. Rev. Lett. **104** (2010) 137001.

BL7U

# Intrinsic Quasi-Particle Dynamics in Topological Metallic States

S. R. Park[1], W. S. Jung[1], G. R. Han[1], Y. K. Kim[1], Ch. Kim[1], D. J. Song[1], Y. Y. Koh[1], C. Kim[1], S. Kimura[2], K. D. Lee[3], N. Hur[3], J. Y. Kim[4], B. K. Cho[4], J. H. Kim[5], Y. S. Kwon[5] and J. H. Han[5]

[1]*EInstitute of Physics and Applied Physics, Yonsei University, Seoul, Korea*
[2]*UVSOR Facility, Institute for Molecular Science, Okazaki 444-8585, Japan*
[3]*Department of Physics, Inha University, Incheon, Korea*
[4]*Department of Materials Science & Engineering, GIST, Gwangju, Korea*
[5]*Department of Physics, Sungkyunkwan University, Suwon, Korea*

Topological metallic (TM) states, the metallic surface states of topological insulator (TI), recently have raised great interest in the condensed matter community because of their novel properties. Spin degeneracy which is normally found in solids is lifted in TM states. Electron spins in TM are locked into the momenta, forming chiral spin states. Such spin texture should strongly suppress backscattering by non-magnetic impurities. Due to these properties, TM states are supposed to have high electron mobilities.

High mobilities in the surface states have not been experimentally measured as the transport method can be used only for bulk conductivity. On the other hand, mobility or life time of surface electrons can be measured by ARPES. To obtain the intrinsic quasi-particle life time, we have performed ARPES experiments on $Bi_2Se_3$, $Bi_2Te_3$ and Sb. $Bi_2Se_3$, $Bi_2Te_3$ and Sb single crystals were grown by flux and Bridgman methods. Samples were cleaved in situ and ARPES measurements were performed at the beamline BL7U [1, 2].

From the earlier experiments at UVSOR, we found out that the quasi-particle dynamics is severely affected by adsorbed atoms and molecules on the surfaces. Therefore, we have raised samples temperatures to anneal off the adsorbed atoms and molecules and obtain clean surfaces. Figure 1 shows ARPES data from $Bi_2Se_3$, $Bi_2Te_3$ and Sb surface states taken with 8 eV photons. 8 eV is found to suppress the bulk state spectral weight. The surface band reaches the Γ point near the 0.3 eV binding energy for $Bi_2Se_3$. This point is called the Dirac point. The binding energies of Dirac points are 0.3, 0.11 and 0.23 eV for $Bi_2Se_3$, $Bi_2Te_3$ and Sb, respectively.

Suppression of the bulk ARPES states allows us to perform reliable self energy analysis on the data. The imaginary parts of the self energies from the data are plotted in Fig. 2. In the data, it is noted that ImΣ from topological surface states are very much energy independent, at around 25 meV. This casts a stark contrast to the case of high temperature superconductors for which ImΣ is very energy dependent. In addition, the width of 25 meV is very small, indicating the quasi-particle life time in the surface states is very long.

Even though 25 meV is already very small, we believe the intrinsic width is even smaller. Generally, electron-electron interaction gives the energy dependent width. Therefore, the constant width indicates that the electron-electron correlation is extremely small. Other contribution to the width may be from the electron-phonon coupling. However, no electron-phonon kink structure was observed, meaning electron-phonon contribution is negligible. Therefore, the only culprit for the breadth is impurity/inhomogeneity. These results clearly show that the intrinsic life time of the quasi-particles in surface states is extremely long, resulting in peak widths of less than a few meV. This value is smaller than any other cases, including the superconducting coherence peak in the ARPES spectrum from the (π,0) point of high temperature superconductors.

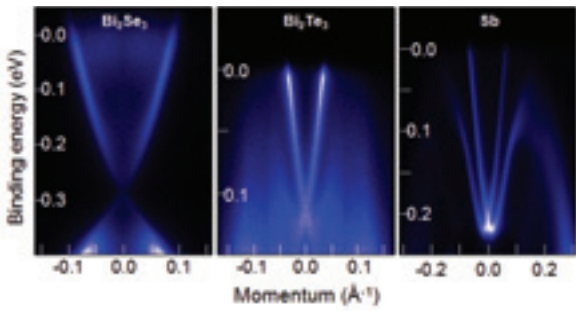


Fig. 1. Near Γ point ARPES data from various topological surface states : (a) $Bi_2Se_3$ (b) $Bi_2Te_3$ and (c) Sb [From ref. 2].

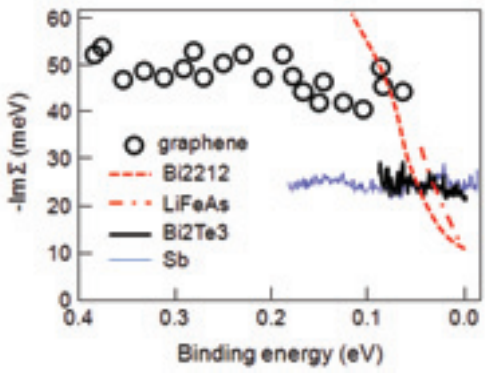


Fig. 2. Plot of ImΣ from $Bi_{2-x}Sn_xTe_3$, Sb, graphene, $Bi_2Sr_2CaCu_2O_{8-\delta}$ (Bi2212) and LiFeAs [From ref. 2].

[1] S. R. Park *et al.*, Phys. Rev. B **81** (2010) 041405.
[2] S. R. Park *et al.*, New J. Phys. **13** (2011) 013008.

BL7U

# Angle-resolved Photoelectron Spectroscopy of HOPG with Photon Energies of <16 eV

S. Tanaka[1], M. Matsunami[2] and S. Kimura[2]

[1]*The Institute of Scientific and Industrial Research, Osaka University, Ibaraki 567-0047, Japan*

[2]*UVSOR Facility, Institute for Molecular Science, Okazaki 444-8585 Japan*

Graphite has been regarded as a "textbook" system for investigations of the solid state physics for many years because of its unique characters. It consists of carbon, which is one of the most basic elements, and the network of the $sp^2$-hybridized orbital makes the quasi-two dimensional electronic structure. The dispersions of the valence band are schematically shown in Fig. 1 [1].

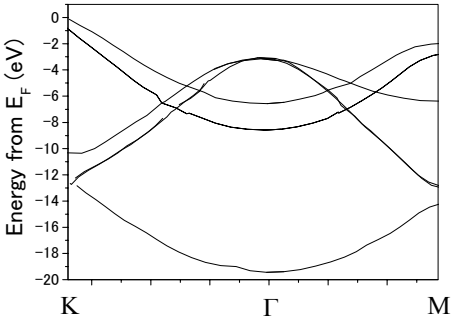


Fig.1 Electronic structure of the graphite.

In this report, we present a photoelectron spectroscopic study of HOPG (Highly Oriente Pyrolytic Graphite) at the photon energy region below 16 eV for the first time.

The experiments were carried out at the BL7U at UVSOR, which covers the photon energy of 6-43 eV, and is equipped with the apparatus for the angle-resolved photoelectron spectroscopy (ARPES). An HOPG sample was cleaved in UHV (<$1x10^{-8}$ Pa), and its fresh surface was investigated. The reliability of the experiments including the sample condition was checked with the comparison of the ARPES spectra taken at $h\nu$=41 eV with the previous result [2].

Figure 2 shows the series of the surface-normal-photoelectron spectra of HOPG at 11 K with photon energies of 7.3-16 eV. Intensities are calibrated by the photon intensities measured with the photodiode. The most striking feature is the sharp peaks just below the Fermi level, whose intensities are resonantly enhanced at $h\nu$=11.2 eV (the width is about 1 eV).

This is surprising since the band of the graphite crosses the Fermi level at the K-point, and the highest occupied state at the Γ-point is about 3 eV below the Fermi level. We found that these peaks are only observed below 30 K of the sample temperature. The resonance is probably due to the excitation into the unoccupied state at 11.2 eV above the Fermi level.

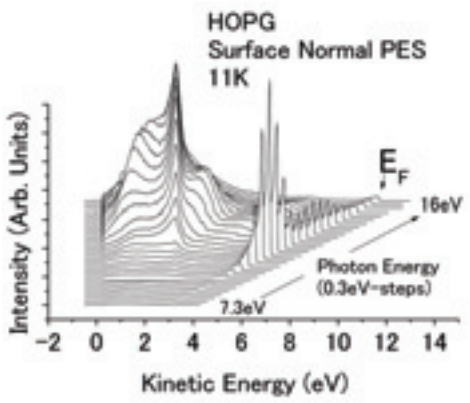


Fig.2 Series of the photoelectron spectra of HOPG.

One may argue that this could be ascribed to an extrinsic origin; the defect or the adsorbed species on the surface. The use of the ARPES, however, enables us to deny this possibility. In Fig. 3, the result of the ARPES at $h\nu$=11.5 eV are shown together with the dispersion of the peak as a function of the $k_{//}$. The dispersion is similar to the calculated one at the K-point along the K-Γ direction of the graphite (solid lines) except a typical quasi-particle behavior.

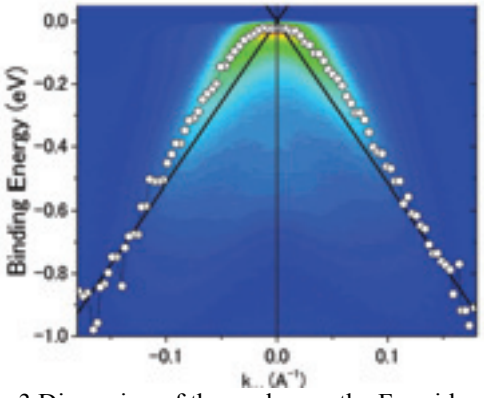


Fig. 3 Dispersion of the peak near the Fermi level.

Most plausible explanation is that the K-point is backfolded to the Γ-point in the two-dimensional Brilloin zone due to the reconstruction of the HOPG lattice which occurs below 30 K. The detailed study to clarify this possibility is now under progress.

[1] R. Ahuja *et al.,* Phys. Rev. B **55** (1997) 4999.
[2] K. Sugawara *et al.,* Phys. Rev. B **73** (2006) 045124.

BL7B

# Characterization of Indium Filter for Generation of Single Order Laser Harmonics

M. Fushitani, A. Matsuda and A. Hishikawa
*Department of Chemistry, Graduate School of Science, Nagoya University, Nagoya 464-8602, Japan*

An ultrashort laser pulse in the extreme ultraviolet (EUV) region is of great interest as a probe to investigate ultrafast dynamics of molecules because of the capabilities of ionizing most atoms and molecules. Among others, laser high-order harmonic generation using a gaseous nonlinear medium is proved to be a promising frequency conversion process to obtain EUV laser pulses [1].

Due to the up-conversion process occurring every half optical cycle of the driving laser pulse, laser high-order harmonics is often generated as a train of pulses, and the corresponding spectrum exhibits a series of odd-order harmonics. For time-resolved measurements, a single pulse is preferred rather than a pulse train. There are several methods to transform a pulse train into a single pulse. A typical method is to employ optical components such as a grating where the harmonics are spectrally dispersed and one of the harmonic orders is spatially selected by using a slit. The single harmonics, however, are significantly stretched in the time domain. An alternative method is to use a thin metal foil as a narrow-band filter. Because of the thickness in the order of $10^3$ Å, less amount of dispersion is introduced in the selected harmonics during the propagation of a metal foil, keeping the pulse duration still short. Here, we investigate the transmission property of an indium foil to obtain ultrashort EUV laser pulse at 80 nm as the 5th order harmonics of the UV laser pulse at 400 nm.

The transmittance of an indium filter with a thickness of 1000 Å was measured at BL7B. The synchrotron radiation (SR) was dispersed by the G2 (600 lines/mm) and G3 (300 lines/mm) gratings in the wavelength range of 40<200 and 120<800 nm, respectively. The reference and transmitted light were detected by a Si photodiode (AXUV100).

Figure 1 shows parts of the transmittance of the indium filter. The maximum transmittance of <10 % is observed around 80 nm with modulations due to the interference effect [2]. The second maximum observed in the region of 150<200 nm is attributed to the second order diffraction of the G2 grating. The transmittance in the 320<480 nm is about 0.1 %.

The expected wavelengths for the 3rd (HH3), 5th (HH5) and 7th (HH7) order harmonics driven by ultrashort laser pulse at 400 nm (UV) are indicated by arrows in Fig. 1. The corresponding transmittances are 0.1 % (UV), 0.07 % (HH3), 10 % (HH5), and 0.3 % (HH7). The present study shows that the indium foil is a suitable narrow-band filter for HH5 to generate ultrashort EUV pulse at 80 nm, with a high contrast ratio ($10^3$) to the neighboring orders (HH3 and HH7).

[1] T. Brabec and F. Krausz, Rev. Mod. Phys. **72** (2000) 545.
[2] W. R. Hunter, D. W. Angel and R. Tousey, Appl. Opt. **4** (1965) 891.

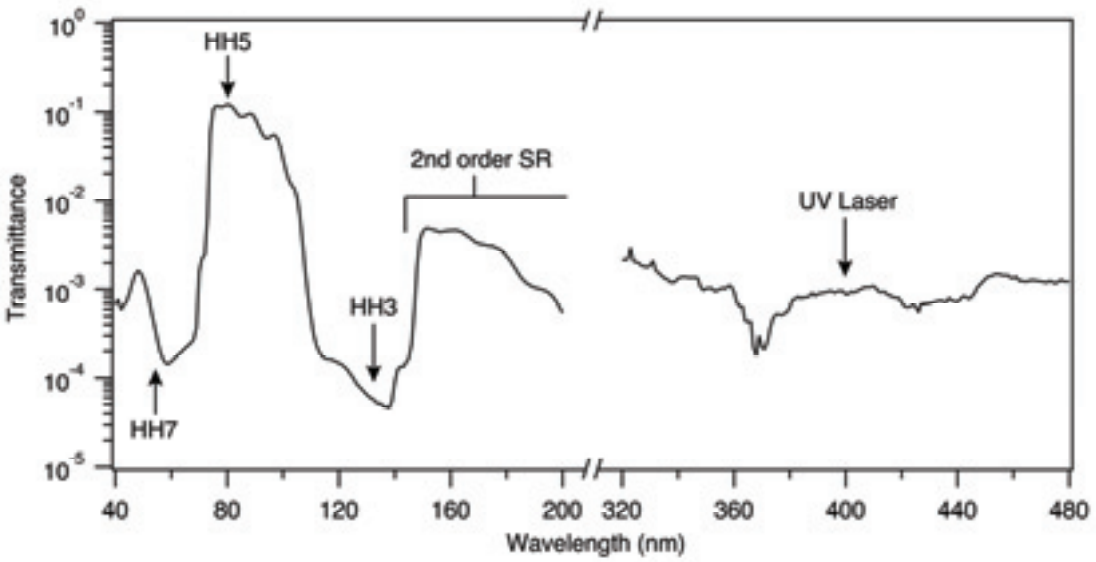


Fig. 1. Parts of the transmittance curve of an indium foil with a thickness of 1000 Å in the wavelength region of 40<200 and 320<480 nm.

BL7B

# Impurity Band of Boron Doped Diamond Observed in the Ultra-Violet Region

T. Inushima[1], Y. Ota[1] and K. Fukui[2]
[1]*Department of Electronics, Tokai University, Hiratsuka 259-1292, Japan*
[2]*Department of Electrical and Electronics Eng., University of Fukui, Fukui 910-8507, Japan*

We report on the refractive index of the impurity band which formed in a semiconductor in the ultra-violet region.

Since the discovery of superconductivity in boron-doped diamond, its impurity band structure has been a key issue for the understanding of the superconductivity. Recently it is reported that when the boron concentration exceeds $N_B$=4×10$^{18}$cm$^{-3}$, impurity band forms at the first excited levels (2p) of the impurity boron at 0.06 eV above the valence band maximum. At higher $N_B$, the wave functions of the 2P states begin to overlap and the impurity band spreads in the *k*-space. Simultaneously, Fermi level rises to the impurity band and a variable range hopping is realized [1]. This mechanism can be seen in the absorption spectra of boron doped diamond, which is shown in Fig. 1.

When $N_B$ is low (<1000 ppm), the prominent absorption peaks are at 0.305 and 0.347 eV, which are the transitions from 1S to 2P$_0$ and 2P$_{\pm1}$ states, respectively. These transitions form a sharp Gaussian shape and are accompanied by LO-phonon sidebands in the higher energy region. When $N_B$ exceeds 4×10$^{18}$ cm$^{-3}$ (2000 ppm), the absorption spectrum changes into a Lorentzian shape governed by the single absorption at 0.35 eV, and the sharp structure disappears, which indicates a drastic decrease of the relaxation time of the excited carriers, or an appearance of the impurity band.

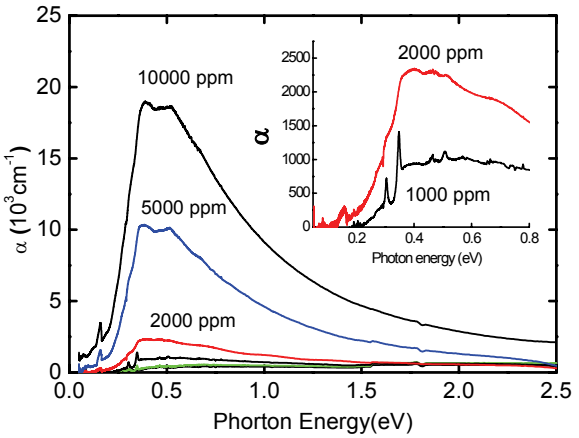


Fig. 1. Boron concentration dependence of the absorption spectra of diamond. The B/C ppm ratio used in the crystal growth is used as the indication of the samples and 10,000 ppm corresponds to $N_B$ of 2×10$^{19}$ cm$^{-3}$.

In order to clarify the energy dependence of the impurity band structure, we measured refractive index of the impurity band in the ultra-violet region using BL7B.

Figure 2 shows the reflection spectra of 2000 ppm boron doped diamond measured at 20 and 300 K by a combination of S2 (6~12 eV) and S3 (3~7 eV) detectors. The spectra have clear sinusoidal interference fringes caused by the transmitting light of the homo-epitaxial diamond film. Using the film thickness of 1.6 μm, refractive index is determined as a function of photon energy, which is shown in the inset of Fig. 2.

The observed refractive index is much smaller than that of the bulk diamond (n~2.4), and shows a minimum at 6 eV. The increase in the higher energy side is due to the direct transition of the bulk diamond at 11.2 eV, and there is no reflection anomaly at the indirect gap at 5.4 eV.

Figure 2 indicates that the impurity band that formed in the bulk diamond has energy dispersion and that it extends up to 10 eV.

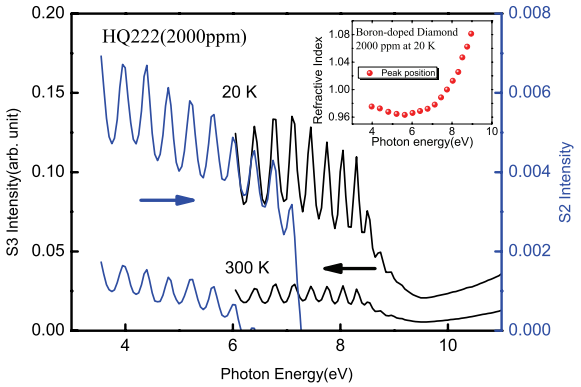


Fig. 2. Reflection spectra of 2000 ppm boron doped diamond at 20 and 300 K. Inset shows the energy dependence of the refractive index.

[1] T. Inushima, R. F. Mamin and H. Shiomi, Phys. Rev. B **79** (2009) 045210.

BL7B

# Spectroscopic Analysis of Electronic States of Solids in Scope of IR-VUV Utilizing BL7B

A. Irizawa[1] and S. Kimura[2,3]

[1]*The Institute of Science and Industrial Research, Osaka University, Ibaraki 567-0047, Japan*

[2]*School of Physical Sciences, The Graduate University for Advanced Studies (SOKENDAI), Okazaki 444-8585, Japan*

[3]*UVSOR Facility, Institute for Molecular Science, Okazaki 444-8585, Japan*

## Introduction

The optical study is one of the most effective approaches in terms of the tunability and the wideness of energy range for understanding of electronic states of solids. The accurate analysis can be achieved from the reflectivity in the wide energy range as far as possible where the optical conductivity can be derived from the reflectivity through Kramers-Kronig (KK) transform. In that sense, the reflectivity data from BL7B in the wide energy range between 1.2 and 40 eV (1000-30 nm) is the important part for KK transform. In this machine time, we prepared several solid samples of strongly correlated *d*-electron system. $Sr_2Ir_{1-x}Rh_xO_4$ (x=0-1) is the newly synthesized system having the perovskite-related crystal structure, so called the Ruddlesden-Popper phase [1]. The end members of this system are that $Sr_2IrO_4$ is the spin-orbital Mott insulator [2, 3] and $Sr_2RhO_4$ is the 2D-like metal [4, 5], respectively. The metal-insulator transition has been reported for the solid solution $Sr_2Ir_{1-x}Rh_xO_4$ where the electronic state will change at around x=0.8. We measured the reflectivities of all these compounds using a 3-m normal incidence monochromator at BL7B in this beam time.

## Experimental

The optical reflectivities of $Sr_2Ir_{1-x}Rh_xO_4$ (x=0-1) were measured at UVSOR-II BL7B. The energy was changed from 1.2 to 40 eV with three gratings (1200, 600, and 300 lines/mm). There are several types of optical window for avoiding the higher degree diffractions. Follow to the former studies in BL7B, we selected the 3 type windows with the 2 gratings for the main experiments. Also we checked the continuity of them by the G2 measurement. The measured temperatures were selected for 300 K and 77 K as a room temperature and the lower temperature.

## Results and Discussion

As a result, the spectra can be obtained for all the compositions of $Sr_2Ir_{1-x}Rh_xO_4$ (x=0, 0.5, 0.8, 1). The measurements were repeated twice for all the compositions. The results are stabilized for the different sequences as shown in Figs. 1 instead of the low intensity of the reflection. Although the connectivity among the spectra with the different gratings and the windows still have some controversial point, they can be connected in the single spectrum by the proportional operation. The temperature variation is hardly discriminated within the limits of error in this experiment.

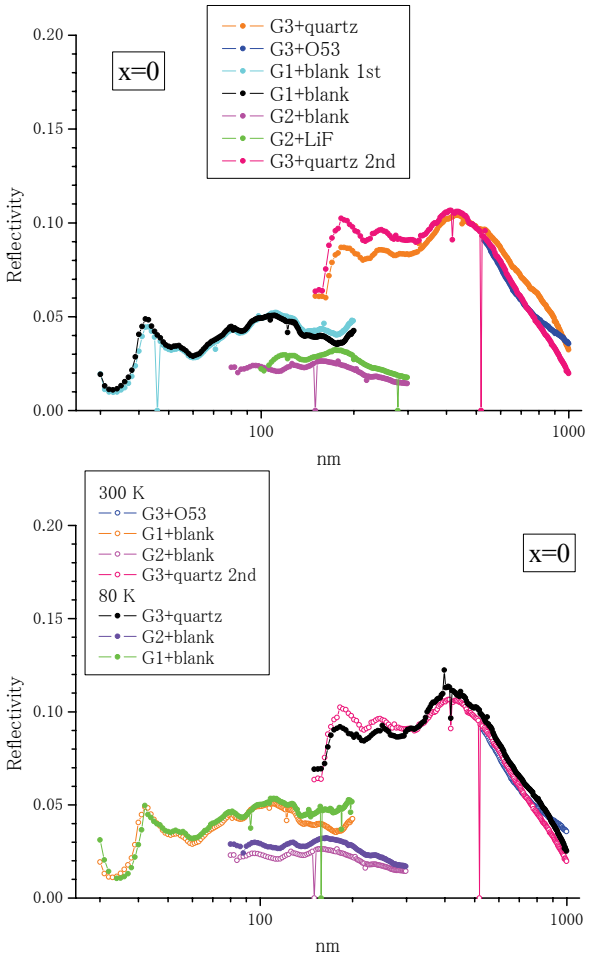


Fig. 1. Stability of reflective spectra for the twice measurements.

[1] M. Isobe, JPS meeting (2010) 24pXP-9.
[2] S. J. Moon *et al.,* Phys. Rev. Lett. **101** (2008) 226402.
[3] B. J. Kim *et al.,* Science **323** (2009) 1329.
[4] F. Baumberger *et al.,* Phys. Rev. Lett. **96** (2006) 246402.
[5] B. J. Kim *et al.,* Phys. Rev. Lett. **97** (2006) 106401.

BL7B

# Optical Study of Rattling Phonons in Clathrate Compounds

T. Mori[1], M. Matsunami[1,2], T. Iizuka[2], S. Kimura[1,2], K. Suekuni[3] and T. Takabatake[3,4]

[1]*UVSOR Facility, Institute for Molecular Science, Okazaki 444-8585, Japan*

[2]*School of Physical Sciences, The Graduate University for Advanced Studies (SOKENDAI), Okazaki 444-8585, Japan*

[3]*Department of Quantum Matter, ADSM and* [4]*Institute for Advanced Material Research, Hiroshima University, Higashi-Hiroshima 739-8530, Japan*

Recently novel phenomena related to local anharmonic phonons observed in cagelike materials such as intermetallic clathrates have attracted much interest [1-4]. In particular, the so-called rattling phonons of guest ions in polyhedral cages and how they may affect such as electric and thermal properties, have been studied extensively in light of their potential application in thermoelectric devices.

Some of the clathrates classified in type-I structure show not only low thermal conductivity with a high thermoelectric figure of merit, but also glasslike temperature dependence of specific heat and thermal conductivity [1]. Such thermal properties are universally observed in glasses or amorphous materials, though the present materials form a regular lattice. It is thus argued that such anomalous thermal behaviors may be caused by the rattling phonons vibrating in an off-centered anharmonic potential.

In this study we measured reflectivity spectra of type-I $Ba_8Ga_{16}Sn_{30}$ ($\beta$-BGS), type-I $Ba_8Ga_{16}Ge_{30}$ (BGG), and type-VIII $Ba_8Ga_{16}Sn_{30}$ ($\alpha$-BGS) to investigate rattling phonon and electric structure. In those materials, only $\beta$-BGS has off-centered rattling phonon and shows glasslike thermal properties.

The single crystals of *n*- and *p*-type $\beta$-BGS, BGG, and $\alpha$-BGS were grown by a self-flux method [1, 2]. Reflectivity spectra of those samples were measured in the photon energy range of 2 meV – 30 eV using several spectroscopies. In the energy range between 2 meV and 1.5 eV, two interferometers (Martin-Puplett and Michelson type) were used. In the energy range between 1.5 and 30 eV, a synchrotron radiation at BL7B in UVSOR facility was used in this machine time. The optical conductivity spectra $\sigma(\omega)$ were calculated from the reflectivity spectra using Kramers-Kronig (KK) relations.

Figure 1 (a) shows obtained reflectivity spectrum of *n*-type $\beta$-BGS at room temperature. The spectrum of each energy region is connected smoothly based on far-infrared spectral data. Optical conductivity spectrum calculated from the reflectivity spectrum using KK relation is shown in Fig. 1 (b). The $\sigma(\omega)$ spectrum of *n*-type $\beta$-BGS consists of mainly three features. Firstly, below about 10 meV, there are four peaks of phonons. The lowest broad peak around 3 meV is assigned as off-center rattling phonon of $Ba(2)^{2+}$ ions. This observation of the rattling phonon is consistent with that obtained by another probe [4]. Secondly, below about 0.1 eV, the Drude-like doped carrier contribution is observed. Thirdly, there are two peaks around 1.5 and 20 eV. Including higher-energy structures, these are due to the electronic interband transitions from valence bands to conduction bands.

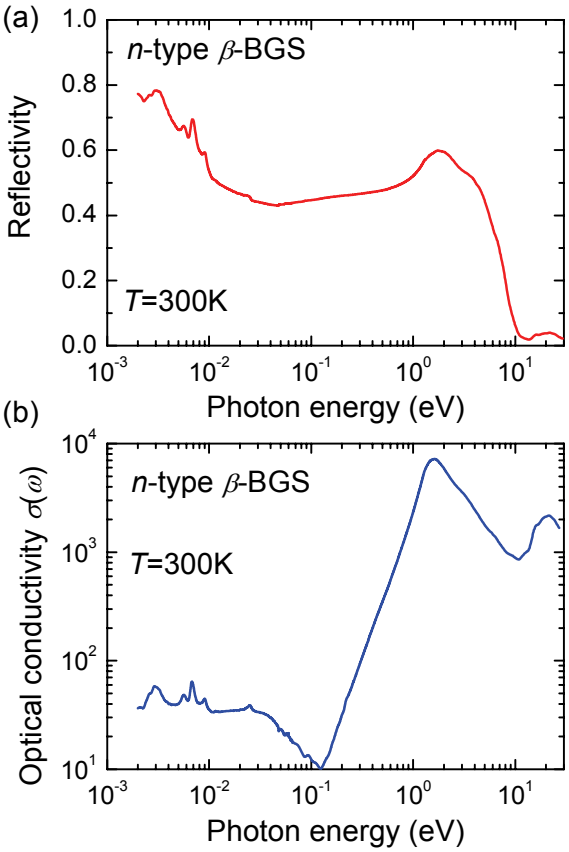


Fig. 1. (a) Observed reflectivity spectra and (b) optical conductivity spectra $\sigma(\omega)$ of *n*-type $\beta$-BGS at room temperature.

[1] M. A. Avila *et al.*, Phys. Rev. B **74** (2006) 125109.
[2] M. A. Avila *et al.*, Appl. Phys. Lett. **92** (2008) 041901.
[3] T. Mori *et al.*, Phys. Rev. B **79** (2009) 212301.
[4] T. Mori *et al.*, Phys. Rev. Lett. **106** (2011) 015501.

BL7B

# Characterization of Wide Bandgap Oxide and Fluoride Crystal in VUV Region

T. Nakazato[1], M. Tsuboi[1], K. Sakai[1], K. Yamanoi[1], T. Shimizu[1], N. Sarukura[1] and T. Fukuda[2]
[1]*Institute of Laser Engineering, Osaka University, Suita 565-0871, Japan*
[2]*WPI-AIMR, Tohoku University, 2-1-1 Katahira, Aobaku, Sendai 980-8577, Japan*

## Introduction

All-solid-state lasers, optics, and scintillators in the vacuum ultraviolet (VUV) region are in demand because of the important roles that they play in various fields. Fluoride and oxide crystals are key materials, which meet these demands because of their wide-bandgap. In our previous research, we proved that zinc oxide (ZnO) is a promising fast scintillator [1], having achieved a luminescence lifetime of less than 100 ps by controlled impurity doping [2]. In this research, we measure the photoluminescence (PL) spectra of two different types of ZnO crystals, undoped and impurity-doped, at various temperatures in order to investigate their optical properties in the VUV region. Results provide the necessary database for optimizing this material for various applications.

## Experiment

We have measured the PL spectra of undoped and impurity-doped ZnO crystals at 20 K, 50 K, 100 K, 150 K, 200 K, 250 K and 300 K. The excitation wavelength was 70 nm.

## Results and Discussion

Figure 1 shows the temperature dependence of the PL spectra. Both the undoped and impurity doped ZnO have two emission peaks at around 380 nm and 600 nm. As shown in Fig. 1 (a), the 380 nm emission peak, which originates from exciton recombination, becomes narrower, more intense, and shifts to a shorter wavelength with decreasing temperature. These indicate that the exciton changes from free exciton to bound exciton with decreasing temperature. On the other hand, shift in wavelength and change in peak width of the 600 nm emission was not observed. Intensity increases with decreasing temperature, reaching maximum at 200 K. However, further decrease in temperature decreases the intensity. The 600-nm emission originates from transition between defect levels in the ZnO crystal. The temperature dependence of the broad emission in the visible region shows a different trend in previous work [3]. Further investigation is being carried out in order to understand this difference. Impurity-doped ZnO also manifests the same temperature dependence, as shown in Fig. 1 (b), except that the intensity of the 600-nm emission reaches maximum at 150 K.

The relative intensity of exciton emission from defect level-transition in impurity-doped ZnO is lower than that in the undoped one. This is because the impurity prevents exciton recombination, wherein

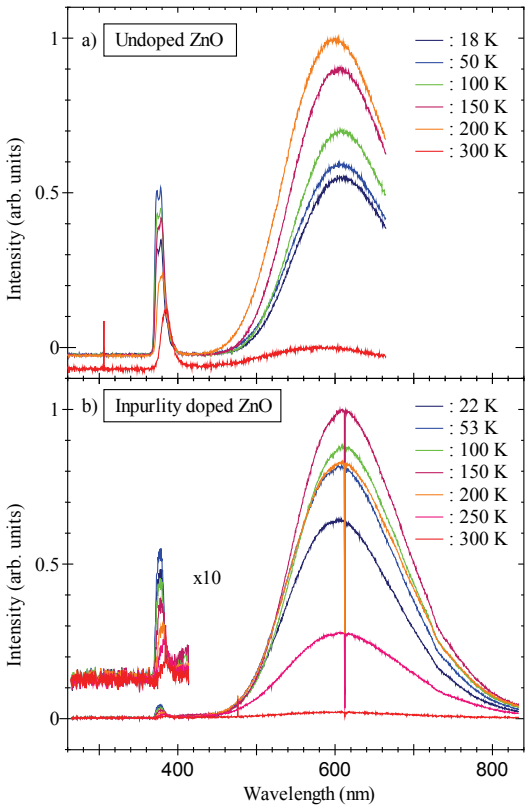


Fig. 1. Photoluminescence spectra of ZnO. Excitation wavelength is 70 nm. a) Undoped ZnO. b) Impurity doped ZnO.

the impurity works as a fluorescence quencher. On the other hand, the wavelength of the emission originating from exciton recombination (380 nm) and from transition between defect levels (600 nm) is the same regardless of impurity doping for all temperatures. These results show that we can control the lifetime without changing emission wavelength and other scintillator properties by impurity-doping. This systematic study will help us in material survey.

[1] M. Tanaka *et al.*, Appl. Phys. Lett. **91** (2007) 231117.
[2] T. Shimizu *et al.*, Rev. Sci. Instrum. **81** (2010) 033102.
[3] H. Mrokoc and U. Ozgur, "Zinc Oxide: Fundamentals, Materials and Device Technology", Wiley-VCH, Weinheim (2009).

BL7B

# Optical Constants of AlN Determined by VUV Ellipsometry

K. Ozaki[1], T. Saito[2], H. Iwai[1], K. Fukui[1] and I. Saito[2]
[1]*Dept. Elec. Elec. Engi, Univ. Fukui, Fukui 910-8507, Japan*
[2]*National Metrology Institute of Japan, National Institute of Advanced Industrial Science and Technology, Tsukuba 305-8563, Japan*

## Introduction

Recently, the need for quantitative measurements of UV-VUV radiation is increasing with the expanding applications of the radiation for sterilization, curing, etc.. However, most-widely used Si photodiodes, have a serious problem of degradation under UV exposure. Therefore, AlN (AlGaN) photodiodes [1] without this problem are attractive. Accurate optical constants of materials composing a detector are necessary for the design and the characterization. Although commercially available spectroscopic ellipsometers are known as a powerful tool to obtain optical constants with high accuracy, the shortest wavelength limit is typically in the near UV region. Among some trials to go down to the VUV range, an AIST group designed a VUV ellipsometer using a oblique incident photodiode as a polarization analyzer and proved that it worked successfully [2]. Currently, we are tuning up the instrument by optimizing various conditions for the use at BL7B. In addition, we tried to obtain optical constants of an AlN by performing VUV spectroscopic ellipsometry measurement to AlN thin films, which can be used for AlN photodiodes.

## Experiment

A VUV ellipsometer used this time is shown in Figure 1. First, the polarizer is not needed in this equipment by the reason that the polarization state of incident light to the sample can be artificially changed by rotating the sample chamber. Due to the characteristics of synchrotron radiation, the incident radiation is nearly linearly polarized. The beam reflected by the sample is detected by an inclined detector, which results in polarization sensitivity. This design eliminates the need of polarizer, which is typically realized by 3-time reflections, and greatly simplifies the mechanism.

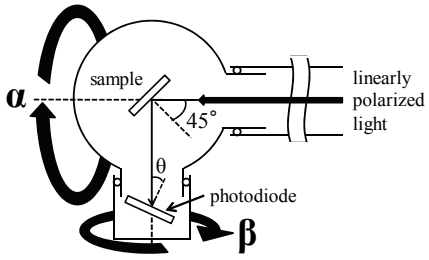


Fig. 1. Schematic layout of a VUV ellipsometer.

## Analysis and Discussion

The Stokes vector **S**' at the detector can be expressed by

$$\mathbf{S}' = \mathbf{M_a}(\Psi_a, \Delta_a)\mathbf{R}(-\beta)\mathbf{M}(\Psi, \Delta)\mathbf{R}(-\alpha)\mathbf{S}, \quad (1)$$

where **S** is the Stokes vector of the incident light to the sample, **M**(Ψ,Δ) the Mueller matrix of a sample, $\mathbf{M}_a(\Psi_a,\Delta_a)$ the Mueller matrix of a detector, **R**(-α) the Muller matrix of a rotator (angle of rotation -α), **R**(-β) the Muller matrix of a rotator (angle of rotation -β). The detector is sensitive only to the intensity component $S'_0$ in **S**'. Hence, the Eq. 1 is expanded on $S'_0$. At certain $\beta$s, the equation is simplified and thus, all Stokes vector component of incident light, Δ, Ψ and $\Psi_a$ are obtained by the fitting to the sample chamber rotation measurement result.

Ellipsometric parameters, Ψ and Δ, were obtained from measurement result of the AlN thin films on $Al_2O_3$ substrate. Complex refractive indeces ($N=n - ik$) of an AlN derived from Ψ and Δ are shown in Figure 2. A red line is a curve calculated by Kramers-Kronig transform and the fitting to reflectance.

In the energy range lower than 9 eV, optical constants obtained had large measurement errors. This is because the optical axis does not match the mechanical axis, which was brought by the change in the position of the incident optical axis depending on the wavelength. This is inevitable due to the spectral design of BL7B. Another cause is the influence of birefringence possibly due to the strain in LiF used for higher-order rejection. In the energy range higher than 9 eV, optical constants of AlN obtained by the ellipsometry are found to be close to those by K-K method considering the error bars.

For better performance, mechanical improvement and measurement automations are planned.

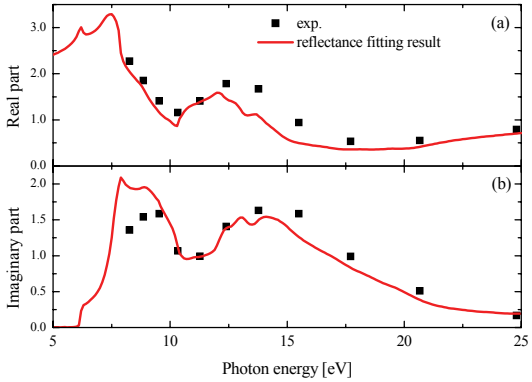


Fig. 2. Complex refractive indices of an AlN, (a) real part and (b) imaginary part.

[1] T. Saito *et al*., Phys. Stat. Solid. C **6** (2009) S658-S661.
[2] T. Saito, M. Yuri and H. Onuki, Rev. Sci. Instrum. **66** (1995) 1570.

BL8B

# Ultraviolet Photoelectron Spectra of Mono-Metal Endohedral Fullerene Er@$C_{82}$ (I)

T. Miyazaki[1], R. Sumii[2,3], H. Umemoto[4], H. Okimoto[4], Y. Ito[4], T. Sugai[4], H. Shinohara[4] and S. Hino[1]

[1] *Graduate School of Science and Engineering, Ehime University, Matsuyama 790-8577, Japan*
[2] *Institutes for Molecular Science, Okazaki 444-858, Japan*
[3] *Research Center for Materials Science, Nagoya University, Nagoya 464-8602, Japan*
[4] *Graduate School of Science, Nagoya University, Nagoya 464-8602, Japan*

Erbium atom entrapped fullerenes have been isolated, the cage symmetry of Er@$C_{82}$ (I) has been determined to be $C_{2v}$ (82:9) by NMR structural analysis, and the oxidation state of Er in Er@$C_{82}$ is an issue worth to investigate. In the current work, the ultraviolet photoelectron spectra (UPS) of Er@$C_{82}$ (I) will be presented.

The ultraviolet photoelectron spectra (UPS) measurement was carried out at the beamline BL8B of Ultraviolet Synchrotron Orbital Radiation Facility (UVSOR) of Institute for Molecular Science. The base pressure of the measurement chamber was $4\times10^{-8}$ Pa, and the pressure during the measurement went up to about $6\times10^{-8}$ Pa. Specimens for UPS measurement were thin films vacuum deposited onto a gold deposited molybdenum disk from a quartz crucible under $5\times10^{-7}$ Pa. The temperature of the crucible during vacuum deposition of Er@$C_{82}$ (I) was 650–700 °C. The UPS were referenced against the Fermi level ($E_F$) of gold and were plotted as a function of binding energy relative to $E_F$.

The upper valence band UPS of Er@$C_{82}$ (I) obtained with $h\nu$ = 20–55 eV incident photons are shown in Fig. 1. Eleven structures labeled A−K and marked with dotted lines were clearly observed. All spectra were normalized by the peak height of the structure E. The intensity of these structures changed, when the incident photon energy was tuned. For example, the intensity ratio of B–D was almost unity at $h\nu$ = 20 eV and 40 eV but changed to about 1:2 at $h\nu$ = 30 eV. This is a typical behavior in the UPS of fullerenes. The spectral onset energy ($E_{onset}$) of Er@$C_{82}$ (I) is 0.38 eV below the Fermi level and this is much smaller than that of empty $C_{82}$ (1.2eV). The UPS of Er@$C_{82}$ (I) in the deeper binding energy region ($E_b$ > 5 eV) is due to ó-electrons that constitute the $C_{82}$ skeletal C–C bonds. The seven peaks in this region were at 5.4 eV (E), 6.8 eV (F), 7.7 eV (G), 8.4 eV (H), 10.1 eV (I), 10.9 eV (J) and 12.9 eV (K). The UPS of the upper binding energy region ($E_b$ < 5 eV) are derived from π-electrons and four structures are observed at 0.7 eV (A), 1.6 eV (B), 2.1 eV (C) and 3.3 eV (D).

The UPS of Er@$C_{82}$ is substantially identical with those of La@$C_{82}$ and Tb@$C_{82}$, which suggests their analogous electronic structure. The upper valence band UPS of Er@$C_{82}$ differs significantly from those of three Tm@$C_{82}$ isomers. This observation supports the empirical rule that the electronic structure of metallofullerenes is governed by the cage structure and the oxidation state of entrapped metal atom: the electronic structure is analogous when the cage structure of metallofullerenes and the oxidation state of the entrapped atom is the same, and the electronic structure might be quite different when the cage structure of the metallofullerenes or the oxidation state of the entrapped atom is different. Using this empirical rule we could deduce the cage structure of metallofullerenes or the oxidation state of the entrapped atom from the UPS measurements. The upper valence band UPS of Er@$C_{82}$ (I) is well reproduced by the simulated spectrum assuming a $C_{2v}$–$C_{82}^{3-}$, confirming the cage structure deduced from NMR analysis. It suggests that Er@$C_{82}$ (I) has the $C_{2v}$–$C_{82}$ cage structure and the oxidation state of the entrapped Er atom is +3.

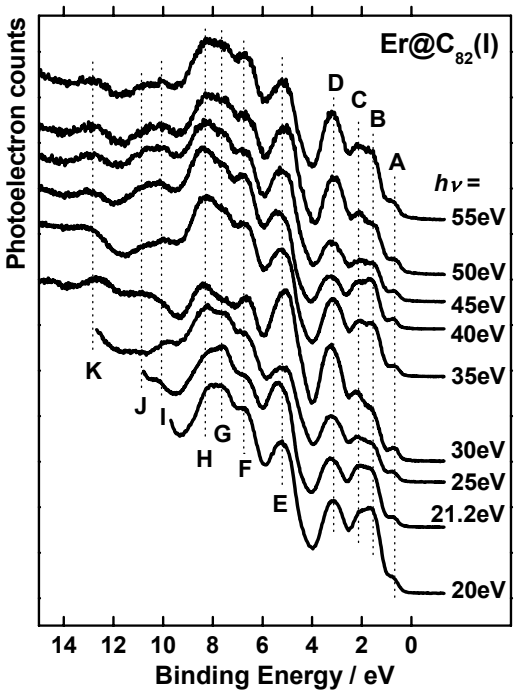


Fig. 1. The incident photon energy dependent UPS of Er@C82 (I) at hν = 20 ~ 55 eV. Eleven structures are observed and their intensity changes upon the tuning of the incident photon energy.